Thiede, J., Myhre, A.M., Firth, J.V., Johnson, G.L., and Ruddiman, W.F. (Eds.), 1996
*Proceedings of the Ocean Drilling Program, Scientific Results,* Vol. 151

# 17. GEOCHEMISTRY AND ORIGIN OF PLIOCENE AND PLEISTOCENE ASH LAYERS FROM THE ICELAND PLATEAU, SITE 907[1]

Christian Lacasse,[2] Martine Paterne,[3] Reinhard Werner,[4] Hans-Joachim Wallrabe-Adams,[4] Haraldur Sigurdsson,[2] Steven Carey,[2] and Guy Pinte[5]

## ABSTRACT

The upper 90 m of sediments from Ocean Drilling Program Leg 151 Site 907 on the Iceland Plateau contain numerous well-preserved volcanic ash layers that provide an excellent record of the source and timing of major Pliocene and Pleistocene explosive eruptions that have occurred in this region. A total of 23 tephra layers and six ash zones were analyzed for major and trace element chemistry and grain size characteristics. Relative ages of the tephra layers were estimated based on paleomagnetic and oxygen isotope stratigraphy. Thicknesses of the ash layers range from less than 1 to 18 cm. It is inferred on the basis of their sorting coefficient and grain size that the majority of the tephra layers are the result of ash fallout from large explosive eruptions. Most of the tephra layers are crystal-poor, with less than 10% total crystal content. Colorless shards dominate over sideromelane (brown glass) and tachylite. Platy bubble wall shards represent the dominant morphological type of glass, with minor amounts of pumice and vesicular shards.

The major element composition of glasses indicates four compositional groups: basalt, basaltic andesite, trachyte and rhyolite. All of the compositionally bimodal tephra layers and the rhyolitic layers have a tholeiitic affinity, compatible with a source from volcanoes in the Pliocene–Pleistocene and upper Pleistocene volcanic rift zones in Iceland. Tephra with alkaline and peralkaline rhyolitic (comendite) glass composition were likely erupted from the only two regions in Iceland having produced transitional and alkali rock series of similar composition: the Snæfellsnes Peninsula and the Eastern Volcanic Zone. Three tephra layers are found to have a trachytic composition, high total alkali concentration, and affinity with the trachy-basaltic rock series of Jan Mayen. All of the basaltic glasses show high potassium concentration (>0.2 wt%), which excludes their origin from the Kolbeinsey Ridge. Rare earth element (REE) patterns from trace element analyses of bulk ash layers indicate various degrees of enrichment in light rare earth elements (LREE) for the silicic tephra, a finding that confirms sources from Iceland and Jan Mayen.

## INTRODUCTION

A 216-m-long sediment sequence was recovered on the Iceland Plateau at Site 907 (69°14.9′N, 12°41.8′W; 1800 m water depth; i.e., around 250 km southwest of Jan Mayen and 350 km northeast of Iceland; Fig. 1). It preserved abundant tephra fall and other volcaniclastic layers (Shipboard Scientific Party, 1995) that are indicators of the volcanic activity in the region for approximately the past 14 m.y. (i.e., from middle Miocene to Holocene). Forty-eight distinct ash layers, each more than 1 cm thick, are identified in all the lithologic units except Unit V. The high core recovery (≥100%) in this sequence enables us to reconstruct the depositional environment of these volcaniclastic layers and provides good age control for individual volcanic events. This study focuses on the Pliocene to Holocene tephra layers recovered from Core 151-907A-1H through Core 151-907A-10H (Table 1). A complementary investigation of the oldest tephra layers of Hole 907A, from Core 151-907A-11H through Core 151-907A-23H (middle and late Miocene) is presented in Werner et al. (this volume).

Among all the Deep Sea Drilling Project (DSDP) and Ocean Drilling Program (ODP) drilling sites in the North Atlantic, Hole 907A is the most proximal to Iceland and likely to contain the most complete record of explosive volcanic events from this hot spot. Analyses have been performed on discrete tephra layers, as well as the ash zones which have been located based on shipboard descriptions (Shipboard Scientific Party, 1995), and downhole measurements of GRAPE density and whole-core magnetic susceptibility (Rack et al., this volume). Electron microprobe analysis of volcanic glass shards and neutron activation (INAA) analysis of bulk ash layers are used to infer potential sources from Iceland, Jan Mayen, and the Kolbeinsey Ridge. Also, an attempt is made to interpret the mode of transport and deposition for the major tephra layers, based on their grain-size characteristics and distance from source. A reconstruction of the timing of explosive volcanic activity is presented in the context of the paleomagnetic and oxygen isotope stratigraphy (Shipboard Scientific Party, 1995; Fronval and Jansen, this volume). However, this record remains subject to the sampling resolution and the non-deposition of ash falls due to the fluctuation of sea ice cover north of Iceland, at least during the Pleistocene, and the change in prevailing wind directions.

## GEOLOGIC SETTING AND PALEOENVIRONMENT OF THE ICELAND PLATEAU

### Morphology and Plate Tectonics

The Iceland Plateau (68°30′N, 12°0′W) is a broad, relatively level platform between Iceland and the Jan Mayen Fracture Zone (transform fault). It is bounded to the west by the Kolbeinsey Ridge (Johnson et al., 1972; Meyer et al., 1972; Johnson, 1974; Vogt et al., 1980) and to the east by the Norway Basin (Fig. 1). Depths across the plateau range from 1800 to 2000 m. Associated with the Iceland Plateau is a 275-km-long and up to 110-km-wide linear ridge, the Jan Mayen Ridge, which strikes in a nearly north–south direction (Fig. 1).

[1]Thiede, J., Myhre, A.M., Firth, J.V., Johnson, G.L., and Ruddiman, W.F. (Eds.), 1996. *Proc. ODP, Sci. Results,* 151: College Station, TX (Ocean Drilling Program).

[2]Graduate School of Oceanography, University of Rhode Island, Narragansett, RI 02882, U.S.A. Lacasse: lacasse@gsosun1.gso.uri.edu

[3]Centre des Faibles Radioactivités, Gif-sur-Yvette, France.

[4]GEOMAR, Research Center for Marine Geosciences, Wischhofstraße 1-3, D-24148 Kiel, Federal Republic of Germany.

[5]Centre d'Etudes Nucléaires de Saclay, Laboratoire Pierre Süe, Gif-sur-Yvette, France.

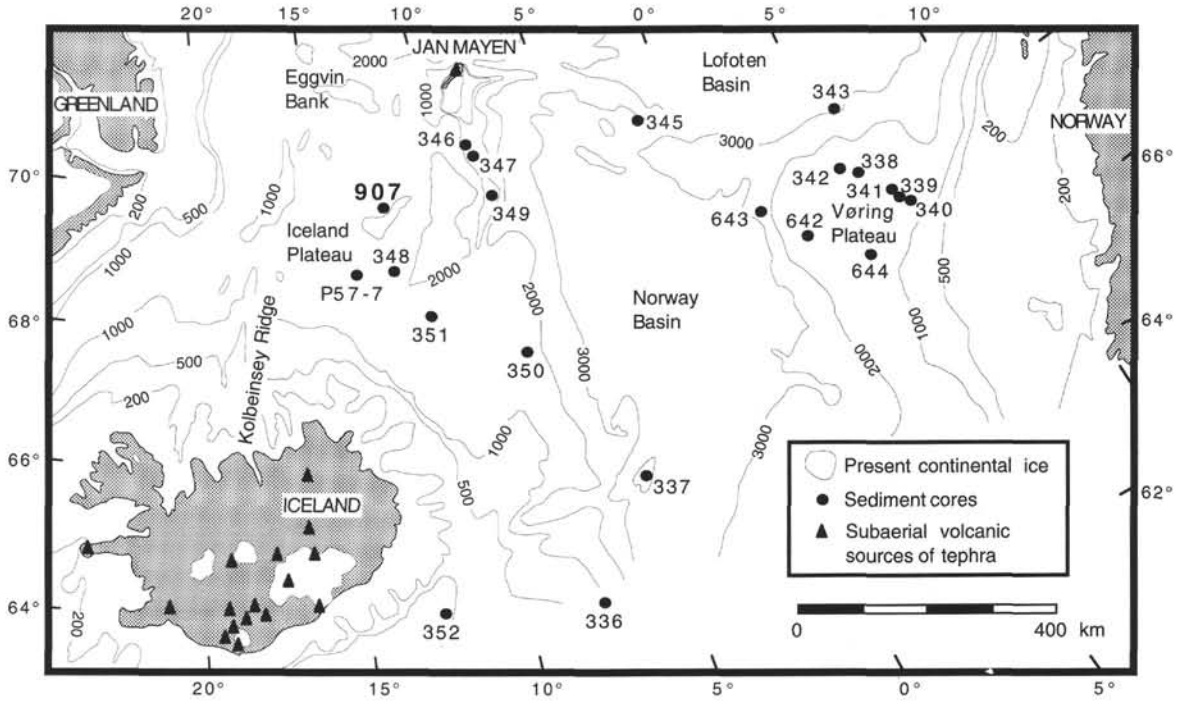


Figure 1. Location map of ODP Leg 151 Site 907 and ODP Leg 104 (Sites 642–644) and DSDP Leg 38 (Sites 336–352) drilling sites. Bathymetric contours in meters. Present continental ice and subaerial volcanic sources of tephra on Jan Mayen and Iceland are shown.

The initial evolution of the region is associated with a complex series of rifting events (rift jumping) giving rise to episodes of intense submarine and subaerial volcanism. Spreading was initiated on the Ægir Ridge in the east, from about 58 Ma through the Eocene and early Oligocene, leading to the formation of the Norway Basin (Talwani and Eldholm, 1977; Myhre and Thiede, 1995). The spreading axis then jumped from the extinct Ægir Ridge to the continental margin of east Greenland, and this resulted in the separation of the Jan Mayen Ridge as a microcontinent from the Scoresby Sund region. Spreading on the Kolbeinsey Ridge was initiated during this rifting episode of the continental Jan Mayen Ridge. Opening continued uninterrupted on the Reykjanes Ridge and Kolbeinsey Ridge. About 20 m.y. ago the rift system moved over the North Atlantic hot spot and led to the separation of rift segments and volcanic zones on the Iceland Platform (Oskarsson et al., 1985).

## Paleoenvironment and Deep-Sea Sedimentation

The present surface oceanic circulation in the area is dominated by a counterclockwise gyre as a result of the East Icelandic Current flowing eastward off north Iceland, the Norwegian Atlantic Current flowing north along the Norway Basin and the East Greenland Current flowing south between the Kolbeinsey Ridge and East Greenland (Kellogg, 1980). Bottom currents on the Iceland Plateau are weak (Damuth, 1978). Oceanic conditions have evolved through time, especially during Pliocene and Pleistocene age, when continental icesheets on Greenland and Iceland were initiated and sea ice cover was common. Oceanic circulation north of Iceland was reconstructed for the Last Glacial Maximum (LGM), 18,000 years ago, based on the study of foraminiferal assemblages in marine sediments (Kellogg, 1980). It shows a weaker East Greenland Current, flowing through the narrow passage between the Greenland and Iceland ice shelves, and the absence of the northern branch of the North Atlantic Current due to the presence of permanent sea-ice west of Iceland. As a result, the counterclockwise circulation, which occurs today over the Iceland Plateau, was almost completely turned off during the LGM and likely during the Pleistocene glacial maxima. On the other hand, the last interglacial, 125,000 years ago, was characterized by a circulation pattern similar to that of today except that the two counterclockwise gyres, initiated by the Jan Mayen and the East Icelandic Currents, were displaced toward the east and were more vigorous (Kellogg, 1980). Oceanic surface circulation evolved between these two extremes during the deposition of the deep-sea tephra of at least Pleistocene age on the Iceland Plateau.

The occurrence of rhyolitic tephra layers in the Iceland Plateau sediments requires explosive volcanism from subaerial or subglacial sources (e.g., Iceland, Jan Mayen), or from shallow submarine sources (e.g., Jan Mayen Bank, Eggvin Bank; Fig. 1). According to the present atmospheric circulation, tephra from large Icelandic eruptions are transported by the prevailing stratospheric winds which are dominantly westerly, just above the tropopause (8–11 km elevation for subpolar latitudes). The distribution of Holocene tephra in surface sediments of the North Atlantic and Norwegian-Greenland Seas supports this airborne dispersal pattern with two lobes extending about 700 km to the east and northeast of Iceland (Kellogg, 1973; Sigurdsson and Loebner, 1981; Sejrup et al., 1989; Sjøholm et al., 1991).

However, very little is known about the evolution of tropospheric and stratospheric paleowind circulation (intensity and direction) in subpolar and polar region during the Pliocene and Pleistocene. Atmospheric General Circulation Model (AGCM) simulations for the Last Glacial Maximum, 18 ka, have been carried out by using boundary-condition changes as specified by CLIMAP (CLIMAP Project Members, 1981; Kutzbach and Wright, 1985; Kutzbach and Guetter, 1986). The simulation for 18 ka indicates that the tropospheric (0–12 km altitude) zonal wind distribution reflects features of the surface temperature distribution, consistent with the thermal wind equation (Kutzbach and Guetter, 1986). Considering especially lower surface temperatures and sea ice extended toward the equator, the model shows that the core of the North Atlantic westerly jet was centered above the southern margin of the North Atlantic sea-ice (at 45°N lat-

itude for January) where the atmospheric temperature gradient was at a maximum. In contrast with stronger westerlies at this mid-latitude (about 5 to 10 $m \cdot s^{-1}$ stronger than today), a local minimum occurred at about 60°N, south of Iceland. Unpublished results of Kutzbach and Guetter for 0 ka and 18 ka stratospheric level up to 32 km altitude indicate limited change in subpolar and polar region in the Northern Hemisphere with slightly stronger winds (J. Merrill, pers. comm., 1996). As suggested before for the oceanic circulation, atmospheric circulation probably evolved between two climate extremes corresponding to interglacial (or present) and glacial conditions (e.g., the LGM at 18 ka) during the Pleistocene period, and therefore these changes should be reflected in the airborne dispersal of tephra.

In addition to airborne fallout deposition of volcanic ash layers, ice-borne sediments (ice-rafted debris [IRD]) dominated the deep-sea terrigenous sedimentation on the Iceland Plateau during at least the last 2.5 m.y. (Shackleton et al., 1984; Jansen and Sjøholm, 1991; Leg 151 Shipboard Scientific Party, 1995). This material originated from the repeated episodes of glacial erosion, which have removed most unconsolidated sediment from the adjacent land areas and inner continental shelves. Low concentrations of fine-grained IRD have been reported from marine cores off mid-Norway and suggest that some North Atlantic glaciations could date back as early as 5.45 Ma (Jansen et al., 1990). The oldest ice-rafted dropstones in the Leg 151 sites were found in the upper Miocene, at about 6.4 Ma, at Site 907 on the Iceland Plateau (Leg 151 Shipboard Scientific Party, 1995). Ice-rafting should be considered, therefore, as another process of dispersal and deposition of ash in the region. Distribution and density of sea ice likely influenced the rate of ice-rafted deposition of tephra.

## DEEP-SEA RECORDS OF ASH LAYERS NORTH OF ICELAND

During DSDP Leg 38 and ODP Leg 104 in the North Atlantic, ash layers of Eocene to Pleistocene age were recovered (Talwani, Udintsev, et al., 1976; Eldholm, Thiede, Taylor, et al., 1987). From petrographic characteristics, Sylvester (1978) inferred several volcanic sources for the ash layers of late Cenozoic and Recent age that have been found in deep-sea cores near Jan Mayen Island (Leg 38, Sites 346–350; Fig. 1). Nearly all consist of well-sorted, fine-grained, highly angular basaltic and felsic glass and mineral fragments (plagioclase, clinopyroxene, orthopyroxene, biotite, hornblende, quartz and opaque mineral: pyrite, titanomagnetite). The relative abundance of tachylite, sideromelane, and clear glass indicates either basaltic, felsic, or bimodal basaltic and felsic composition. They are petrographically similar to volcanic rocks of comparable ages in the nearby volcanic centers of Iceland and Jan Mayen. However, a few tephra samples of early Cenozoic age from the outer Vøring Plateau (Site 338) and the Lofoten Basin (Site 345) show a different mineralogical composition, and are likely derived from separate and unknown sources, possibly the presently submerged portions of the Kolbeinsey and Mohns Ridges, or even the Iceland-Faeroe Ridge. Based on the morphologic and granulometric characteristics of the tephra, Sylvester (1978) suggested a phreatomagmatic eruption type with atmospheric transport.

The first chemical analyses of silicic tephra recovered on Leg 38 were presented in Sigurdsson and Loebner (1981) and Loebner (1982). These studies revealed two prominent compositional series, which were erupted throughout the Cenozoic. The first, low-K series, ranging from icelandites through dacites and rhyolites, is depleted in Al and enriched in Fe and Ca. The second, high-K and high-Al series, ranges from quartz-trachytes to alkali rhyolites and associated comendites. Four apparent episodes of Tertiary explosive volcanism were inferred from the distribution of volcanic ash layers (i.e., normalized frequency of occurrence) cored during Leg 38 and their chemistry: middle Eocene (Iceland-Faeroe Ridge), middle Oligocene (Kialineq region, East Greenland), early to middle Miocene (emergence of the Iceland platform), and Pliocene and Pleistocene (rift jumping and development of the volcanic zones in Iceland). In contrast, Donn and Ninkovitch (1980) inferred only two major epochs of explosive volcanism during the middle Eocene and Pliocene from the same DSDP records and North Atlantic piston cores. Their analysis suggests that the Cenozoic ash layers derived from subaerial sources in Iceland. These two interpretations regarding the frequency of explosive volcanism in the North Atlantic are limited by hiatuses in the sedimentary record, poor core recovery, and drilling disturbance of sediments in most of the Leg 38 sites.

Leg 104 on the Vøring Plateau, northeast of Iceland, was the second DSDP/ODP Leg in the North Atlantic (Eldholm, Thiede, Taylor, et al., 1987). Forty-five ash layers were found in Neogene to Holocene sediments recovered at Sites 642–644 (Fig. 1). Excellent core recovery (79%–98%) and freshness of the glass allowed for a detailed study of their distribution, chemical characteristics, and origin (Bitschene et al., 1989; Desprairies et al., 1989). Most of these layers, up to several centimeters thick, consist mainly of fresh rhyolitic glass. About one-fourth of the ash layers contain variable amounts of more basic glass shards, which range in composition from Mg-rich tholeiites to icelandites through poor Mg-poor basalts, ferrobasalts, and tholeiitic andesites. Desprairies et al. (1989) separated the ash layers into three compositional groups: homogeneous or subhomogeneous, heterogeneous (acidic/intermediate), and heterogeneous (acidic/basic) layers. The homogeneous or subhomogeneous ash layers are exclusively rhyolitic or predominantly rhyolitic but extending toward Icelandic compositions. The heterogeneous (acidic/intermediate) layers are predominantly rhyolitic but also show an intermediate (andesitic to icelanditic) component separated by a significant chemical gap from the rhyolites. The heterogeneous (acidic/basic) layers were subdivided into two subgroups according to the proportions of the two end-members and the intermediate compositions.

$TiO_2$ and FeO* vs. MgO plots were used to study the chemical variation within heterogeneous layers (Desprairies et al., 1989). The trends shown are typically tholeiitic and are characterized by an increase of $SiO_2$ and alkalis with decreasing MgO concentration. FeO* and $TiO_2$ contents increase from Mg-rich basalts to ferrobasalts and decrease in the more Mg-poor glasses. For the bimodal layers in which the basic end-member is ferrobasaltic, the intermediate compositions plot near the tie-lines connecting the composition of the two end-members. However, when the basic end-member is truly basaltic (Mg-rich), the intermediate glass shards plot above these tie-lines and are usually enriched in $TiO_2$ and FeO* with respect to the basaltic end-member. From this last observation, Desprairies et al. (1989) concluded that the intermediate glass composition of these latter ash layers cannot be derived from simple magma mixing (hybridization) but rather from fractional crystallization. They suggested that most of the heterogeneous ash layers resulted from the ejection of the upper (rhyolitic) to intermediate (ferrobasaltic) levels of density-stratified magma chambers intruded by ascending basaltic magma (Sigurdsson and Sparks, 1981). Trace element data on bulk ash layers indicate that all the tephra of bimodal composition, as well as most of Neogene rhyolitic ash levels (low-K type), belong to LREE-enriched tholeiitic series (Desprairies et al., 1989). High-K rhyolitic ash levels, on the other hand, show distinct geochemical features indicative of a different source.

Two periods of intense volcanic activity were inferred by Desprairies et al. (1989) from the frequency of ash layers: the early/middle Miocene boundary (14–16 Ma) and the late Miocene (7–8 Ma). All the chemically heterogeneous ash layers and the low-K rhyolitic ash levels were attributed to Icelandic sources, whereas the high-K rhyolitic ash horizons possibly originated from other subaerial sources (East Greenland, Jan Mayen Ridge). No relationship between the age of the tephra and their degree of alteration (palagonite, smectite, glauconite) was found.

Besides their geochemistry, the mineralogy and grain-size characteristics of the ash layers recovered during Leg 104 were documented by Bitschene et al. (1989). Median grain sizes of the ashes are about 100 μm, and maximum grain sizes range up to 1200 μm. All ash layers are well sorted and represent distal fallout from major explosive eruptions. Crystals and lithics are minor constituents (<2% by volume) for the majority of the tephra. The rhyolitic tephra comprise mainly phenocrysts of plagioclase, zircon, and clinopyroxene. Plagioclase and clinopyroxene phenocrysts and opaques minerals are present in the basaltic ash layers. Quartz (mostly detrital), amphibole, and biotite occur occasionally.

## METHODS

### Sampling Resolution and Sample Preparation

All the discrete ash layers that have been identified in Core 151-907A-1H through Core 151-907A-10H by the Shipboard Scientific Party (1995) were sampled for grain size and chemical analysis. Layers thicker than 10 cm were sampled at the bottom and top, whereas only a single sample was taken from thinner layers (Table 1). This sampling resolution was subsequently increased following the GRAPE bulk density and whole-core magnetic susceptibility measurements of the sediment (Rack et al., this volume). Most of the volcaniclastic deposits in the upper 50 m (terrigenous sediment with dominant ice-rafted detritus) are characterized by low density and high magnetic susceptibility relative to background sediment. In the lower part of the sequence, however, they are typically of higher density as a result of the dominant biogenic component of the sediment. Other horizons occurring as dispersed ash (ash zones) were found and sampled (Table 1).

Each sample of bulk sediment was dried and weighed. Its carbonate fraction was removed by hydrochloric acid. The carbonate-free residue was rinsed and wet-sieved through a set of screens (1 phi unit interval) down to 5.5 phi (22 μm).

### Grain-Size and Modal Analyses

Each sieved fraction (>5.5 phi) was dry-weighed. The remaining fine fraction was analyzed using an automated Elzone 150+ particle analyzer, with a 48-μm orifice and a conducting solution of sodium pyrophosphate (4%). This instrument uses the electrosensing technique to determine particle size and can detect particles down to 1 μm in size. The combined method of wet sieving and Elzone particle analysis thus allows analysis of sediment with a large grain size range. Grain-size characteristics (median and mean sizes, sorting, and skewness) were derived from the cumulative granulometric curve (Folk, 1974; Table 1).

Abundance of the different glass and mineral components was estimated by counting about 300–500 grains under the microscope (Table 1). This analysis was carried out on the 62.5–125 μm or 125–250 μm fractions, which contain the most representative and reliable material for mineral determination. The glass components were divided into several groups: colorless shards, brown glass or sideromelane, and tachylite. Minerals such as quartz (mainly detrital), plagioclase, clinopyroxene, olivine, and amphibole were counted, as well as lithics and siliceous biogenic material (radiolarians and diatoms).

### Electron Microprobe Analysis

All microprobe analyses of glass shards were performed on the coarse fraction >62.5–125 μm or >125–250 μm. The major element composition of volcanic glass particles was determined at a specific depth interval in each ash layer and ash zone (about 15 and 30 individual analyses of glass shards for a homogeneous and a heterogeneous glass composition, respectively) using a Cameca electron microprobe. The analytical technique follows the recommendations adopted for the standardization of the chemical analysis of tephra (INQUA Inter-Congress Committee on Tephrochronology, 1990). A beam current of 10 nA with an accelerating voltage of 15 kV was used. Na loss was minimized for silicic glass analysis by using a beam defocussed to 10 μm and by collecting counts at regular time intervals (2 s) and extrapolating the decay curve back to count initiation (Nielsen and Sigurdsson, 1981). Calibration of silicic and basaltic glass compositions was made by analyzing the natural glass standards KN-18 (comendite obsidian from Kenya; Nielsen and Sigurdsson, 1981) and VG-2 (basaltic glass from the Juan de Fuca Ridge).

### Analysis by Neutron Activation

Neutron activation was performed on bulk ashes for all the discrete ash layers with less than 5%–10% crystals. Each tephra sample (31–62 μm or 62–125 μm fraction) was irradiated with a flux of $10^{14}$ n/cm$^2$/s for 1 to 3 hours in aluminum sleeves at the Centre d'Etudes Nucléaires of Saclay, France. Measurements of trace element concentrations were made using an intrinsic Ge detector of 100 cm$^3$, using granite and basalt rocks standards (GSN and BEN) from the CRPG (Centre de Recherches Pétrographiques et Géochimiques) of Nancy, France. Quantification was done following automatic peak search, nuclear identification, and calculation for element concentration. Analytical precision is 10% for Sc, Co, Zr, Cs, La, Ce, Sm, Eu, Tb, Yb, Hf, Ta, and Th; 15% for Cr, Sb, Ba, Nd, and Lu; and 20% for U.

## LITHOLOGY AND STRATIGRAPHY

Ash layers were recovered from lithologic Units I, II, and III, which were identified in the Pliocene and Pleistocene sediment sequence of Site 907 based on their varying amounts of biogenic and siliciclastic material, and volcanic glass. A detailed lithologic description of these units is presented in Shipboard Scientific Party (1995). The sediments are unlithified and dark grayish brown silty clay and clayey silt, with scattered dropstones (>0.5 cm) throughout the sequence. Lithologic Unit I (Sections 151-907A-1H-1, 0 cm, through 151-907A-2H-CC, 31 cm; 0–16.8 meters below seafloor or mbsf) is distinguished by the presence of abundant foraminifers. Lithologic Unit II (Sections 151-907A-3H-1, 0 cm, to 151-907A-7H-1, 150 cm; 16.8–56.3 mbsf) is characterized by the absence of biogenic carbonate and silica and an enrichment in silt- and sand-sized siliciclastic grains. Lithologic Unit III (Sections 151-907A-7H-0, 0 cm, through 151-907A-13H-6, 30 cm; 56.3–118.1 mbsf) was defined by the presence of biogenic silica, a downcore increase in volcanic glass content, and a decrease in quartz and feldspar abundance. The base of Unit III is marked by an upcore increase in quartz and is accompanied by the first appearance of ice-rafted dropstones.

Interpretation of Unit III (late Miocene to Pliocene) indicates a transitional phase with a progressive replacement of biogenic silica-rich sediment with ice-rafted debris (IRD). Unit II (Pliocene to Quaternary) is thought to represent the bulk of the Quaternary with the beginning of a glacial regime as early as 3 Ma (at about 57–58 mbsf). Unit I (Quaternary) was interpreted to be the record of the last 0.8 m.y. with the Brunhes/Matuyama boundary (0.78 m.y.) occurring at about 16.15 mbsf (Shipboard Scientific Party, 1995). This uppermost sequence consists of dominantly glacial sediments (IRD) interrupted by episodic deposition of carbonate-rich layers (foraminifer-bearing sediments) corresponding to interglacials. The uppermost 23 cm of Core 151-907A-1H, is enriched in calcareous microfossils and represents the Holocene.

## DATING OF TEPHRA LAYERS

Relative ages of the marine tephra deposits were estimated based on their position within the chronostratigraphy provided by the paleomagnetic reversal record and the $\delta^{18}O$ record (Shipboard Scientific

**Table 1. Depth, paleomagnetic and $\delta^{18}O$ dating, thickness, grain-size characteristics and composition of ash layers and ash zones of Hole 907A.**

| Layer | Core, section, interval (cm) | Depth (mbsf) | Paleomag. age (ka) | $\delta^{18}O$ age (ka) | Type | Color | Thickness (cm) | Top–bottom (mbsf) | Grain-size characteristics | | | | Glass | | Tach./opaq. (3) (%) | Plagio./ K feld. (4) (%) | Cpx. (5) (%) |
|---|---|---|---|---|---|---|---|---|---|---|---|---|---|---|---|---|---|
| | | | | | | | | | Ø50 | Mz | Sg | Sk | Col. (1) (%) | Sid. (2) (%) | | | |
| A | 1H-1, 26–27 | 0.26 | 13 | 11.57 | DA | | | | | | | | | | | | |
| B | 1H-2, 50–51 | 2.00 | 97 | 122.26 | DA | | | | | | | | | | | | |
| C | 1H-3, 53–55 | 3.53 | 170 | 204.64 | AL | very dark gray | <5.0 | 3.50–3.55 | 5.77 | 5.80 | 2.18 | 0.02 | 94 | 1 | | | 1 |
| D* | 1H-3, 61–63 | 3.61 | 177 | 211.80 | AL | very dark gray | 18.0 | 3.56–3.74 | 5.00 | 5.06 | 1.73 | 0.05 | 97 | 2 | | | |
| D* | 1H-3, 71–73 | 3.71 | 177 | 211.80 | AL | very dark gray | | | 3.73 | 4.08 | 1.61 | 0.32 | 95 | 4 | | | |
| E* | 2H-3, 97–99 | 11.27 | 545 | 642.00 | AL | gray | 10.0 | 11.20–11.30 | 5.27 | 5.21 | 1.59 | –0.06 | 92 | 2 | 6 | | |
| E* | 2H-3, 100–102 | 11.30 | 545 | 642.00 | AL | gray | | | 5.23 | 5.21 | 1.53 | –0.02 | 80 | 8 | 9 | 2 | |
| F | 2H-3, 118–119 | 11.48 | 554 | 648.13 | DA | | | | | | | | | | | | |
| G | 2H-6, 139–141 | 16.19 | 789 | 774.10 | AL | black | 10.0 | 16.10–16.20 | 3.64 | 3.85 | 1.55 | 0.20 | 58 | 39 | 1 | | |
| H* | 3H-4, 47–49 | 21.77 | 1176 | | AL | dark grayish brown | 10.0 | 21.75–21.85 | 4.09 | 4.27 | 1.87 | 0.15 | 99 | | 1 | | |
| H* | 3H-4, 52–54 | 21.82 | 1176 | | AL | dark grayish brown | | | 3.50 | 3.89 | 1.77 | 0.33 | 98 | | 1 | | |
| I | 3H-6, 118–120 | 25.48 | 1354 | | AL | grayish olive | 11.0 | 25.40–25.51 | 4.36 | 4.54 | 1.87 | 0.15 | 86 | | 7 | 3 | |
| J | 4H-1, 17–18 | 26.47 | 1402 | | DA | | | | | | | | | | | | |
| K | 5H-4, 36–38 | 40.66 | 2141 | | AL | very dark gray | 18.0 | 40.61–40.79 | 4.23 | 4.39 | 1.48 | 0.17 | 76 | 19 | 4 | | |
| L | 6H-6, 111–113 | 53.91 | 2848 | | AL | dark gray | 1.0? | 53.87–53.88 | 3.95 | 4.23 | 1.87 | 0.22 | 98 | 1 | 1 | | |
| M | 7H-3, 96–97 | 58.76 | 3096 | | DA | | | | | | | | | | | | |
| N | 7H-4, 86–88 | 60.16 | 3167 | | AL | dark gray | 2.0 | 60.15–60.17 | 3.14 | 3.68 | 1.78 | 0.46 | 98 | 1 | 1 | | |
| O | 7H-5, 21–23 | 61.01 | 3209 | | AL | black–brown | 8.0 | 60.95–61.03 | 3.82 | 4.15 | 2.00 | 0.25 | 30 | 1 | | 29 | |
| P | 7H-5, 90–92 | 61.70 | 3244 | | AL | black | 4.0 | 61.69–61.73 | 3.68 | 4.13 | 1.91 | 0.36 | 51 | 17 | 29 | | |
| Q | 7H-6, 120–122 | 63.50 | 3341 | | AL | black | <1.0 | 63.50–63.50 | 6.43 | 6.35 | 1.96 | –0.06 | 53 | 29 | 9 | 1 | |
| R* | 7H-6, 131–133 | 63.61 | 3350 | | AL | grayish brown | 10.0 | 63.60–63.70 | 5.18 | 5.33 | 1.82 | 0.12 | 98 | | | 1 | |
| R* | 7H-6, 137–139 | 63.67 | 3350 | | AL | grayish brown | | | 4.50 | 4.63 | 1.80 | 0.11 | 98 | | | | |
| S | 8H-1, 1–3 | 64.31 | 3392 | | AL | gray | 8.0 | 64.30–64.38 | 4.82 | 5.03 | 1.87 | 0.17 | 99 | | | | |
| T | 8H-3, 97–98 | 68.27 | 3773 | | DA | | | | | | | | | | | | |
| U | 8H-4, 39–41 | 69.19 | 3915 | | AL | black | 2.0 | 69.20–69.22 | 4.14 | 4.27 | 1.66 | 0.12 | | 50 | 49 | 1 | |
| V | 8H-6, 120–122 | 73.00 | 4462 | | AL | black | 2.0 | 73.00–73.02 | 2.73 | 3.94 | 3.05 | 0.60 | 35 | 6 | 52 | 6 | 2 |
| W | 9H-2, 39–41 | 75.69 | 4751 | | AL | dark gray? | 2.0 | 75.67–75.69 | 5.91 | 5.85 | 2.18 | –0.04 | 98 | | 1 | | |
| X | 9H-3, 35–37 | 77.15 | 4907 | | AL | dark gray? | 5.0 | 77.11–77.16 | 3.50 | 4.38 | 2.46 | 0.54 | | 33 | 52 | 11 | 2 |
| Y | 9H-4, 52–54 | 78.82 | 5050 | | AL | | ? | | 6.00 | 6.08 | 1.98 | 0.06 | 83 | 1 | | 1 | |
| Z | 9H-6, 64–66 | 81.94 | 5241 | | AL | dark gray? | 5.0 | 81.93–81.98 | 4.59 | 4.86 | 1.64 | 0.25 | 2 | 31 | 66 | | 1 |
| AA | 9H-6, 102–104 | 82.32 | 5264 | | AL | | 4.0 | 82.30–82.34 | 5.36 | 5.45 | 2.00 | 0.07 | 100 | | | | |
| AB | 9H-6, 115–117 | 82.45 | 5272 | | AL | | 6.0 | 82.44–82.50 | 3.55 | 3.85 | 1.59 | 0.28 | 100 | | | | |
| AC* | 10H-1, 148–150 | 84.78 | 5415 | | AL | gray | 18.0 | 84.75–84.93 | 6.09 | 6.24 | 1.27 | 0.18 | 25 | 39 | 23 | 9 | 3 |
| AC* | 10H-2, 0–2 | 84.80 | 5415 | | AL | gray | | | 5.18 | 5.33 | 1.59 | 0.14 | 100 | | | | |

Notes: * = ash layer sampled at two depth intervals. DA = dispersed ash, AL = ash layer. Ø50 = median size, Mz = graphic mean, Sg = sorting coefficient, Sk = graphic skewness, after Folk (1974). (1) Colorless glass shards (platy and vesicular) and micropumice; (2) sideromelane (brownish glass); (3) tachylite and opaque; (4) plagioclase and K feldspar; (5) clinopyroxene.

Party, 1995; Fronval and Jansen, this volume). Mean paleomagnetic and $\delta^{18}O$ ages were determined by linearly interpolating between magnetic reversals and isotopic stage boundaries, respectively (Table 1; Fig. 2).

Paleomagnetic analysis of Hole 907A shows a very well defined polarity stratigraphy down to 95 mbsf, allowing a precise age control for this depth interval. The magnetozones were identified and correlated with the geomagnetic polarity time scale (GPTS) of Cande and Kent (1992) (Shipboard Scientific Party, 1995). The paleomagnetic record of the upper 90 m spans the last 5.7 m.y. down to the Miocene/Pliocene boundary.

The oxygen isotope stratigraphy was primarily based on planktonic foraminifers (*N. pachyderma* left) for the upper 20 m of the sequence, and agrees very well with the benthic isotope data and carbonate data (Fronval and Jansen, this volume). Stage boundaries and reference ages were derived from the SPECMAP time scale (Imbrie et al., 1984) for the upper Pleistocene and from the new orbital tuned age scale of Shackleton et al. (1990) for the lower Pleistocene. This

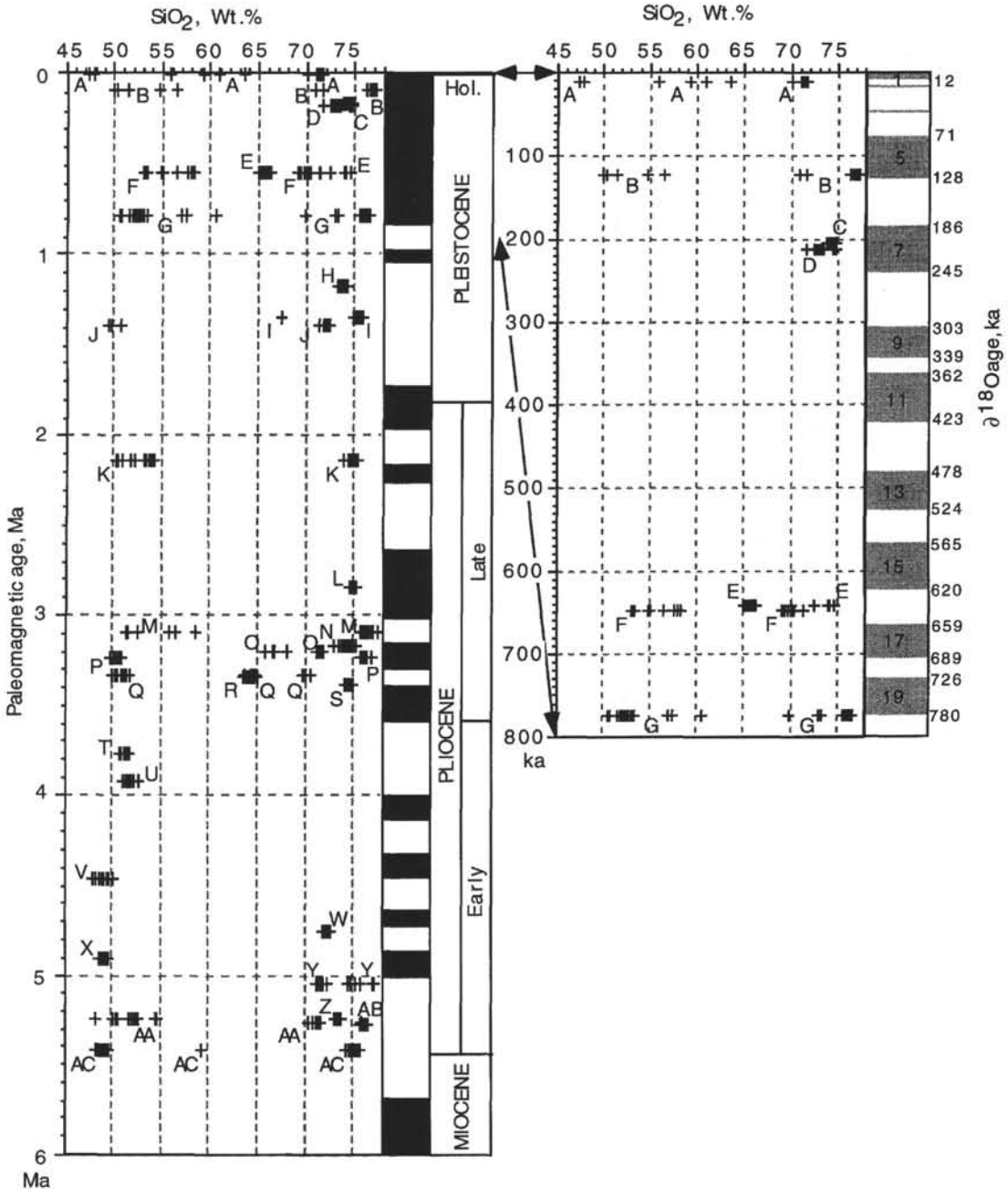


Figure 2. Stratigraphic position and silica content of glasses of Pliocene and Pleistocene ash layers in Hole 907A. Paleomagnetic and $\delta^{18}O$ ages are from Shipboard Scientific Party (1995) and Fronval and Jansen (this volume), respectively. Geomagnetic polarity time scale (GPTS) after Cande and Kent (1992). Isotopic stage boundaries and reference ages after Imbrie et al. (1984) for the upper Pleistocene and Shackleton et al. (1990) for the lower Pleistocene.

record spans the last 780 k.y. down to Stage 21, just below the Brunhes/Matuyama boundary.

## DESCRIPTION AND GRAIN-SIZE CHARACTERISTICS OF TEPHRA LAYERS

Two major types of tephra occurrence (ash layer: type AL; and dispersed ash: type DA) within the sediment were defined, based on their visual characteristics and modal composition, and were labelled A through AC (Table 1). The ash layers were found having a sharp basal contact and an upward fining. They are characterized by high magnetic susceptibility. Dispersed ashes (ash zones) were also found over depth intervals of several tens of centimeters. Twenty-three discrete ash layers (type AL) were studied along the depth interval of 0–85 mbsf, which corresponds to the Pliocene and Pleistocene periods (Shipboard Scientific Party, 1995). The intervals commonly have normal grading, with a sharp basal contact and a gradual upper contact that shows evidence of mixing by bioturbation. Thickness varies from ≤1 cm (layers L and Q) to 18 cm (layers D, K, and AC) (Table 1). Although they are easily identified in the sediment, some ash layers are extensively burrowed, making it difficult to estimate their thickness (e.g., layer C, between 3.50 and 3.55 mbsf). Ash color varies from black to gray, with brown, olive, or green hues. The darkness of the ash layers appears to depend mainly on the amount of pyrite and pyrite-coated shards rather than on the amount of brown glass. All these layers are identified by peaks in the magnetic susceptibility of the sediment, with values exceeding $200 \times 10^{-6}$ cgs for layers E, G, H, I, O, X, Z, and AC. High peaks of magnetic susceptibility result from an abundance of magnetite-bearing crystals, basaltic components (sideromelane and tachylite), or pyrite-coated shards.

Most of the ash layers are crystal-poor, with less than 10% of crystals, with the exception of layers E-base (9% feldspar, 2% clinopyroxene), O (29% feldspar, 12% amphibole), X (11% feldspar, 2% clinopyroxene), and AC-top (9% feldspar, 3% clinopyroxene). Other minerals such as olivine (e.g., up to 2% in layer AC-top), quartz (essentially detrital), magnetite, and pyrite are present in minor amounts in some layers. Colorless shards are dominant over brown shards (sideromelane) and tachylite grains (Table 1). Morphologically, platy bubble wall shards are dominant over pumice and vesicular shards. Layers C, D, E, H, L, N, R, S, W, AA, AB, and AC-base contain up to 90% or more of colorless shards and can be considered as exclusively silicic. Layers U, X, and Z are essentially basic in composition with more than 85% of sideromelane and tachylite. Between these two compositional end-members, several ash layers were found to be heterogeneous in composition; the ratio of silicic glass shards over sideromelane and tachylite ranges between 10:1 (layer E-base) and 1:2.5 (layer AC-top).

Tephra also occur as dispersed glass shards (type DA) over several tens of centimeter depths within the sediment, showing high glass shard concentration in the silt and sand-size fraction. These ash-rich intervals, or ash zones, could not be observed visually but showed up on the magnetic susceptibility record. Several of these horizons were sampled and analyzed for their glass chemistry (layers A, B, F, J, M, and T) (Table 1).

Grain-size characteristics of the discrete ash layers (type AL) were determined, including median diameter (Ø50), graphic mean (*Mz*), graphic standard deviation (*Sg*, sorting coefficient), and graphic skewness (*Sk*) (Folk, 1974; Table 1). The first two represent the overall size of the ash particles, Ø50 varying closely with *Mz* (Table 1). The majority of the Site 907 layers fall into the very fine sand and coarse silt size classes, between 3 and 5 phi (Folk, 1974). Several layers were found to be finer (layers C, Q, Y, W, and AC-top), close to 6 phi. Most of the *Sg* values range between 1.5 and 2.0, indicative of relatively good sorting, which likely took place as ash particles settled through the water column (Fig. 3). Based on the pyroclastic fall deposit field of Walker (1971) shown in Figure 3, only layer V at Site 907 shows granulometric characteristics incompatible with a primary fallout origin from a submarine or subaerial volcanic source. Layer V is the coarsest tephra (Ø50: 2.73 phi) observed in the sediment sequence and is poorly sorted (*Sg:* 3.05). In the thick layers D, H, R, mainly, and AC, normal grading is observed between the bottom and

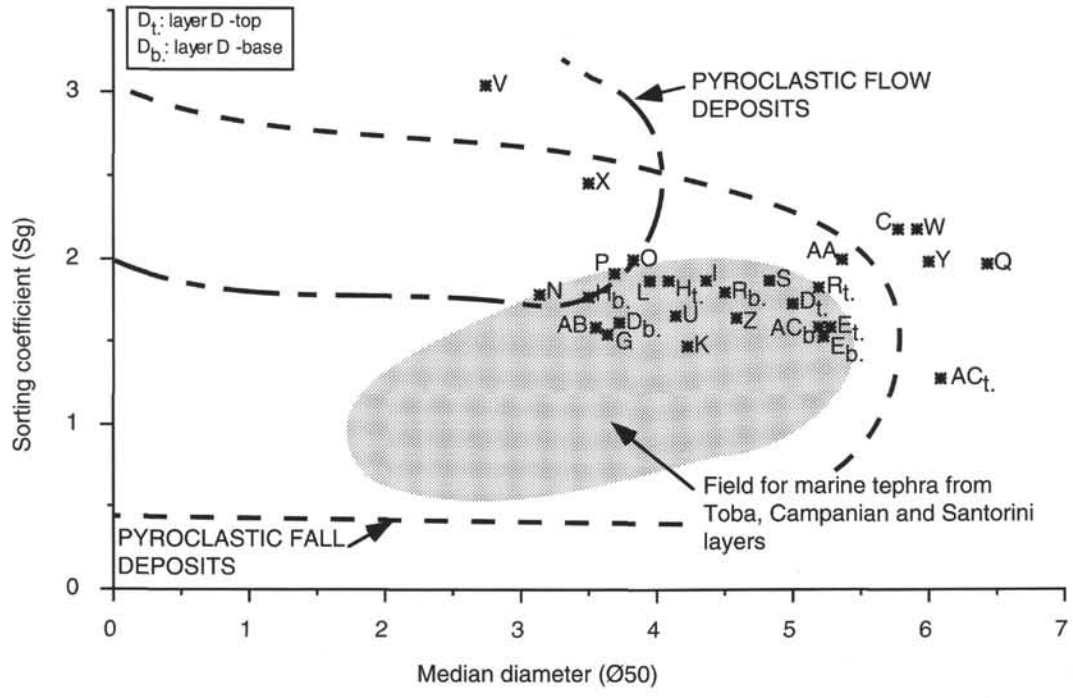


Figure 3. Median grain size (Ø50) vs. sorting coefficient (Sg) for deep-sea tephra layers in Hole 907A. Fields of pyroclastic flow deposits and pyroclastic fall deposits are from Walker (1971). Marine tephra field from Toba, Campanian, and Santorini layers is from Ninkovich et al. (1978).

the top of the layers. It can be interpreted as the result of extensive size fractionation in the water column (Table 1). Figure 3 also shows that most of the ash layers of Site 907 plot in the upper half of the *Sg-Ø50* field for marine tephra from several large eruptions (Toba, Campanian, Santorini), with distances from source ranging between 400 and 2500 km (after Ninkovich et al., 1978). This last observation agrees with a likely airborne transport of these ashes from volcanic sources located on Iceland and Jan Mayen, approximately 350–650 km south and 250 km north of Site 907, respectively.

## GEOCHEMISTRY AND SOURCES OF TEPHRA LAYERS

### Major Elements

Colorless glass shards are the most abundant glassy components in the ash layers of Site 907 (Table 1). Microprobe analytical totals of analyses of silicic glass range from 93% to 99%, with the difference from 100% attributed largely to the water content of the glass (Table 2). Totals for the basaltic to intermediate glass range between about 98% and 101% (Table 3). Half of the 29 ash horizons studied are chemically homogeneous, with a distinct basic (layers T, U, V, X with 47 to 52 wt% $SiO_2$) or acid composition (layer R with 63–65 wt% $SiO_2$; layers C, D, H, I, L, N, S, W, Y, V, Z, AB with 69–78 wt% $SiO_2$) (Fig. 2). The other half of the layers are characterized by a heterogeneous glass composition ranging between basic, intermediate, and acid (layers A, B, F, G, J, K, M, P, Q, AA, AC with $SiO_2$ of 47–78 wt%), or exclusively acid (layers E and O with $SiO_2$ of 63–75 wt%).

The total alkali-silica (TAS) diagram (Le Bas et al., 1986) was used to classify glass shard compositions (Fig. 4). All of the tephra plot within the four major TAS fields defining basalt, basaltic andesite, trachyte, and rhyolite compositions (Fig. 4). Figure 4 shows TAS fields of Holocene and upper Pleistocene rock series from Iceland and Jan Mayen defined by their whole-rock composition, after Jakobsson (1979a) and Imsland (1984), respectively. Rhyolitic te-

**Table 2. Electron microprobe analyses and normative composition of silicic glassy tephra from Hole 907A.**

| Core, section: | 1H-1 | 1H-2 | 1H-2 | 1H-3 | 1H-3 | 1H-3 | 2H-3 | 2H-3 | 2H-3 | 2H-3 | 2H-6 |
|---|---|---|---|---|---|---|---|---|---|---|---|
| Interval (cm): | 26–27 | 50–51 | 50–51 | 53–55 | 61–63 | 71–73 | 97–99 | 97–99 | 100–102 | 118–119 | 139–141 |
| Layer: | A | B | B | C | D* | D* | E* | E* | E* | F | G |
| Type: | DA | DA | DA | AL | AL | AL | AL | AL | AL | DA | AL |
| N: | 12 | 10 | 2 | 15 | 6 | 10 | 3 | 3 | 8 | 12 | 12 |
| $SiO_2$ | 70.31 (0.46) | 73.79 (1.66) | 69.60 (0.55) | 71.28 (0.53) | 70.88 (1.06) | 71.53 (0.69) | 61.73 (0.40) | 70.67 (0.40) | 62.67 (0.60) | 66.05 (0.84) | 72.80 (0.64) |
| $TiO_2$ | 0.27 (0.05) | 0.23 (0.11) | 0.49 (0.14) | 0.24 (0.04) | 0.40 (0.05) | 0.41 (0.07) | 0.74 (0.08) | 0.37 (0.31) | 0.67 (0.11) | 0.31 (0.06) | 0.22 (0.04) |
| $Al_2O_3$ | 13.31 (0.30) | 11.04 (0.39) | 11.96 (0.09) | 11.94 (0.11) | 8.83 (0.77) | 8.73 (0.60) | 16.08 (0.20) | 12.92 (0.25) | 16.35 (0.18) | 14.70 (0.26) | 11.29 (0.15) |
| FeO* | 3.94 (0.14) | 2.78 (0.98) | 5.93 (0.13) | 3.35 (0.13) | 6.05 (0.42) | 6.05 (0.40) | 2.18 (0.18) | 1.17 (0.07) | 2.21 (0.32) | 1.50 (0.10) | 2.69 (0.14) |
| MnO | 0.14 (0.05) | 0.06 (0.06) | 0.18 (0.03) | 0.11 (0.05) | 0.23 (0.05) | 0.27 (0.08) | 0.17 (0.06) | 0.20 (0.07) | 0.18 (0.07) | 0.22 (0.04) | 0.10 (0.05) |
| MgO | 0.21 (0.02) | 0.03 (0.03) | 0.06 (0.04) | 0.08 (0.02) | 0.02 (0.01) | 0.01 (0.01) | 0.60 (0.03) | 0.25 (0.33) | 0.58 (0.12) | 0.17 (0.03) | 0.04 (0.02) |
| CaO | 1.30 (0.07) | 1.50 (0.49) | 3.08 (0.04) | 1.81 (0.09) | 0.32 (0.02) | 0.31 (0.04) | 1.36 (0.08) | 0.70 (0.66) | 1.48 (0.16) | 0.54 (0.08) | 1.32 (0.13) |
| $Na_2O$ | 5.75 (0.30) | 4.83 (0.32) | 4.78 (0.05) | 4.83 (0.26) | 6.37 (0.37) | 6.31 (0.41) | 5.07 (0.19) | 4.96 (0.04) | 5.41 (0.34) | 5.92 (0.26) | 4.40 (0.17) |
| $K_2O$ | 3.46 (0.08) | 1.84 (0.11) | 1.53 (0.10) | 2.37 (0.08) | 4.02 (0.11) | 4.00 (0.12) | 5.84 (0.22) | 4.64 (0.13) | 5.90 (0.13) | 5.32 (0.24) | 2.69 (0.09) |
| Total | 98.69 | 96.10 | 97.61 | 96.01 | 97.12 | 97.62 | 93.77 | 95.88 | 95.45 | 94.73 | 95.55 |
| Q | 19.64 | 36.00 | 28.07 | 30.28 | 30.05 | 30.93 | 6.12 | 23.50 | 4.72 | 11.82 | 34.58 |
| Or | 20.56 | 11.25 | 9.16 | 14.49 | 24.19 | 23.95 | 36.62 | 28.51 | 36.35 | 33.06 | 16.54 |
| Ab | 48.94 | 42.30 | 41.00 | 42.29 | 23.48 | 22.95 | 45.54 | 42.26 | 47.74 | 48.40 | 38.76 |
| An | 0.30 | 3.12 | 6.76 | 4.04 | | | 4.12 | | 3.04 | | 3.25 |
| Ne | | | | | | | | | | | |
| Di | 5.44 | 4.07 | 7.77 | 4.65 | 1.44 | 1.39 | 2.55 | 3.09 | 3.88 | 2.45 | 3.17 |
| Hy | 2.87 | 1.55 | 3.72 | 2.26 | 8.90 | 8.91 | 2.49 | 0.77 | 1.88 | 1.58 | 2.04 |
| Ol | | | | | | | | | | | |
| Mt | 1.67 | 1.21 | 2.53 | 1.46 | | | 0.98 | | 0.97 | | 1.18 |
| Il | 0.52 | 0.45 | 0.95 | 0.47 | 0.78 | 0.79 | 1.50 | 0.73 | 1.33 | 0.62 | 0.44 |
| Total | 99.94 | 99.96 | 99.96 | 99.95 | 99.96 | 99.96 | 99.92 | 99.94 | 99.92 | 99.92 | 99.95 |

| Core, section: | 3H-4 | 3H-4 | 3H-6 | 4H-1 | 5H-4 | 6H-6 | 7H-3 | 7H-4 | 7H-5 | 7H-5 | 7H-6 |
|---|---|---|---|---|---|---|---|---|---|---|---|
| Interval (cm): | 47–49 | 52–54 | 118–120 | 17–18 | 36–38 | 111–113 | 96–97 | 86–88 | 21–23 | 90–92 | 120–122 |
| Layer: | H* | H* | I | J | K | L | M | N | O | P | Q |
| Type: | AL | AL | AL | DA | AL | AL | DA | AL | DA | AL | AL |
| N: | 8 | 8 | 15 | 12 | 15 | 15 | 11 | 16 | 10 | 15 | 4 |
| $SiO_2$ | 71.04 (0.51) | 70.85 (0.44) | 71.94 (0.42) | 69.38 (0.40) | 71.86 (0.69) | 71.91 (0.28) | 72.83 (0.53) | 71.43 (0.74) | 67.54 (0.59) | 72.93 (0.37) | 67.93 (0.22) |
| $TiO_2$ | 0.19 (0.04) | 0.19 (0.06) | 0.23 (0.05) | 0.20 (0.04) | 0.20 (0.06) | 0.17 (0.03) | 0.16 (0.05) | 0.38 (0.09) | 0.11 (0.04) | 0.21 (0.03) | 0.46 (0.01) |
| $Al_2O_3$ | 12.33 (0.08) | 12.21 (0.16) | 9.62 (0.12) | 13.43 (0.25) | 11.71 (0.13) | 11.84 (0.10) | 11.88 (0.25) | 12.11 (0.18) | 13.92 (0.19) | 11.40 (0.13) | 7.86 (0.09) |
| FeO* | 2.60 (0.12) | 2.65 (0.13) | 3.76 (0.15) | 3.01 (0.12) | 2.84 (0.24) | 2.83 (0.10) | 2.15 (0.21) | 2.50 (0.24) | 1.84 (0.09) | 2.18 (0.08) | 8.44 (0.12) |
| MnO | 0.11 (0.06) | 0.08 (0.03) | 0.13 (0.05) | 0.10 (0.05) | 0.10 (0.04) | 0.11 (0.03) | 0.06 (0.03) | 0.13 (0.05) | 0.13 (0.05) | 0.10 (0.04) | 0.37 (0.06) |
| MgO | 0.01 (0.01) | 0.00 (0.00) | 0.01 (0.01) | 0.05 (0.01) | 0.03 (0.05) | 0.05 (0.02) | 0.01 (0.01) | 0.30 (0.07) | 0.05 (0.01) | 0.10 (0.01) | 0.02 (0.02) |
| CaO | 0.64 (0.05) | 0.64 (0.04) | 0.24 (0.04) | 0.85 (0.05) | 0.96 (0.14) | 1.19 (0.05) | 1.26 (0.09) | 1.34 (0.14) | 0.56 (0.06) | 1.02 (0.06) | 0.47 (0.05) |
| $Na_2O$ | 5.78 (0.26) | 5.90 (0.29) | 5.24 (0.23) | 5.54 (0.27) | 5.33 (0.26) | 4.80 (0.25) | 4.57 (0.23) | 5.27 (0.31) | 5.10 (0.34) | 4.74 (0.25) | 7.49 (0.56) |
| $K_2O$ | 3.55 (0.14) | 3.49 (0.10) | 4.07 (0.10) | 3.66 (0.11) | 2.78 (0.16) | 2.99 (0.05) | 2.24 (0.06) | 2.61 (0.11) | 5.06 (0.19) | 2.97 (0.11) | 3.95 (0.09) |
| Total | 96.25 | 96.01 | 95.24 | 96.22 | 95.81 | 95.89 | 95.16 | 96.07 | 94.31 | 95.65 | 96.99 |
| Q | 24.25 | 24.39 | 33.12 | 20.85 | 28.56 | 30.17 | 35.51 | 28.17 | 17.59 | 32.55 | 26.02 |
| Or | 21.68 | 21.36 | 25.07 | 22.34 | 17.05 | 18.32 | 13.84 | 15.97 | 31.57 | 18.26 | 23.71 |
| Ab | 45.14 | 44.95 | 27.97 | 48.43 | 46.46 | 42.12 | 40.45 | 46.18 | 45.58 | 41.74 | 18.74 |
| An | | | | 1.01 | | 2.01 | 5.54 | 1.75 | 0.16 | 1.11 | |
| Ne | | | | | | | | | | | |
| Di | 2.92 | 2.93 | 1.11 | 2.97 | 4.40 | 3.65 | 0.89 | 4.44 | 2.45 | 3.66 | 2.11 |
| Hy | 2.65 | 2.66 | 5.56 | 2.63 | 1.69 | 2.10 | 2.45 | 1.60 | 1.54 | 1.25 | 12.57 |
| Ol | | | | | | | | | | | |
| Mt | | | | 1.31 | 1.09 | 1.24 | 0.95 | 1.09 | 0.82 | 0.96 | |
| Il | 0.37 | 0.37 | 0.46 | 0.39 | 0.40 | 0.34 | 0.32 | 0.75 | 0.22 | 0.42 | 0.89 |
| Total | 99.94 | 99.94 | 99.95 | 99.94 | 99.95 | 99.95 | 99.95 | 99.95 | 99.93 | 99.95 | 99.96 |

phra is by far the most abundant and they have an Icelandic affinity. Two rhyolite layers (F and Q) are unusually rich in alkali. Three layers (E, Q, and R) have a composition similar to the Jan Mayen volcanic system, and show the highest $Na_2O+K_2O/SiO_2$ ratios (0.19–0.21), uncommon among Icelandic silicic rock series. For comparison, a maximum ratio of 0.15 was found in a trachytic pumice (tephra Sn3, unpubl. data) from the alkalic volcano Snæfellsjökull in western Iceland (Jóhannesson et al., 1981). For layers with relatively homogeneous basic or intermediate glass compositions (layers F, G, K, P, Q, T, U, V, X, Z, and AC; see Table 2), basalt and basaltic andesite are the two dominant types, with a few shards in layer G showing a more evolved icelandite composition (Fig. 4). Layers X, V, and AC show more basic composition, with $SiO_2$ ranging between 48 and 49.5 wt%. All the other layers having a basaltic and basaltic andesitic affinity plot outside the Jan Mayen rock series field and well within the Iceland field.

## Basic and Intermediate Glass

Figures 5, 6, and 7 show composition of individual basic and intermediate glass shards for three different geological periods (Pleistocene, late and early Pliocene). CaO vs. MgO plots show a single trend with a negative correlation for the three time intervals. $SiO_2$, $Al_2O_3$, and FeO* show a weak trend with MgO concentration, defining separate clusters, for the Pleistocene and the early Pliocene (Figs. 5, 7). A low-Fe, high-Si and Al trend is indicated by the glass composition of layers F and J (Pleistocene) and layers T, U, and Z (early Pliocene). In contrast, layers B and G (Pleistocene) and layers V, X, and AC (early Pliocene) define a high-Fe, low-Si and Al trend. No separate trends can be observed from the major element chemistry of the late Pliocene layers (Fig. 6). Only the composition of layer Q, with high Al and Ca and low Fe, can be distinguished from the general trend observed. The most primitive glass composition was found

**Table 2 (continued).**

| Core, section: | 7H-6 | 7H-6 | 7H-6 | 8H-1 | 9H-2 | 9H-4 | 9H-4 | 9H-4 | 9H-6 | 9H-6 | 9H-6 |
|---|---|---|---|---|---|---|---|---|---|---|---|
| Interval (cm): | 120–122 | 131–133 | 137–139 | 1–3 | 101–103 | 52–54 | 52–54 | 52–54 | 64–66 | 102–104 | 115–117 |
| Layer: | Q | R* | R* | S | W | Y | Y | Y | Z | AA | AB |
| Type: | AL | AL | AL | AL | AL | AL | AL | AL | AL | AL | AL |
| N: | 5 | 9 | 8 | 14 | 15 | 6 | 5 | 3 | 8 | 13 | 15 |
| $SiO_2$ | 62.14 (0.59) | 61.17 (0.68) | 61.49 (0.30) | 70.40 (0.31) | 69.48 (0.38) | 67.74 (0.48) | 70.82 (0.27) | 72.64 (0.59) | 70.02 (0.37) | 67.98 (0.78) | 72.47 (0.37) |
| $TiO_2$ | 0.67 (0.07) | 0.67 (0.05) | 0.66 (0.07) | 0.18 (0.05) | 0.34 (0.04) | 0.33 (0.05) | 0.18 (0.07) | 0.09 (0.08) | 0.61 (0.07) | 0.29 (0.05) | 0.09 (0.03) |
| $Al_2O_3$ | 16.88 (0.22) | 16.69 (0.17) | 16.70 (0.19) | 12.49 (0.14) | 11.12 (0.10) | 12.62 (0.13) | 12.33 (0.35) | 11.58 (0.11) | 12.27 (0.15) | 12.04 (0.20) | 12.30 (0.16) |
| FeO* | 2.21 (0.05) | 2.31 (0.10) | 2.28 (0.10) | 1.60 (0.10) | 4.69 (0.21) | 3.74 (0.25) | 2.02 (0.26) | 1.06 (0.03) | 2.45 (0.17) | 4.20 (0.13) | 1.53 (0.07) |
| MnO | 0.20 (0.06) | 0.18 (0.04) | 0.18 (0.04) | 0.07 (0.03) | 0.16 (0.05) | 0.11 (0.03) | 0.07 (0.02) | 0.03 (0.02) | 0.09 (0.05) | 0.14 (0.06) | 0.04 (0.04) |
| MgO | 0.38 (0.03) | 0.36 (0.02) | 0.35 (0.03) | 0.11 (0.02) | 0.01 (0.01) | 0.21 (0.02) | 0.08 (0.03) | 0.01 (0.01) | 0.37 (0.04) | 0.01 (0.01) | 0.08 (0.01) |
| CaO | 0.87 (0.18) | 0.81 (0.06) | 0.77 (0.06) | 0.59 (0.04) | 0.51 (0.04) | 1.93 (0.17) | 1.40 (0.25) | 0.67 (0.05) | 1.36 (0.06) | 0.67 (0.05) | 1.23 (0.07) |
| $Na_2O$ | 7.20 (0.45) | 7.16 (0.38) | 7.05 (0.30) | 4.12 (0.22) | 6.36 (0.27) | 5.03 (0.13) | 4.65 (0.17) | 4.21 (0.15) | 5.12 (0.25) | 6.10 (0.19) | 4.62 (0.28) |
| $K_2O$ | 5.88 (0.35) | 5.67 (0.19) | 5.68 (0.20) | 4.94 (0.19) | 3.44 (0.11) | 2.77 (0.11) | 2.86 (0.17) | 3.83 (0.19) | 2.94 (0.11) | 3.83 (0.18) | 2.77 (0.09) |
| Total | 96.43 | 95.02 | 95.16 | 94.50 | 96.11 | 94.48 | 94.41 | 94.12 | 95.23 | 95.26 | 95.13 |
| Q | | | | 27.02 | 23.71 | 23.72 | 30.72 | 33.78 | 26.62 | 19.89 | 33.18 |
| Or | 35.86 | 35.08 | 35.10 | 30.77 | 20.96 | 17.20 | 17.82 | 23.98 | 18.15 | 23.57 | 17.14 |
| Ab | 52.74 | 53.29 | 54.30 | 36.76 | 39.26 | 44.73 | 41.50 | 37.75 | 45.27 | 42.31 | 40.95 |
| An | | | | 1.06 | | 3.87 | 4.57 | 1.48 | 1.90 | | 4.87 |
| Ne | 1.69 | 1.94 | 1.35 | | | | | | | | |
| Di | 3.82 | 3.62 | 3.44 | 1.77 | 2.33 | 5.44 | 2.43 | 1.82 | 4.40 | 3.09 | 1.34 |
| Hy | | | | 1.48 | 6.25 | 2.68 | 1.65 | 0.49 | | | 1.61 |
| Ol | 1.44 | 1.62 | 1.64 | | | | | | 1.31 | 5.15 | |
| Mt | | | | 0.71 | | 1.66 | 0.90 | 0.47 | 1.08 | | 0.68 |
| Il | 1.32 | 1.34 | 1.31 | 0.36 | 0.67 | 0.66 | 0.36 | 0.18 | 1.21 | 0.58 | 0.18 |
| Total | 99.92 | 99.92 | 99.92 | 99.94 | 99.95 | 99.95 | 99.95 | 99.94 | 99.95 | 99.94 | 99.95 |

| Core, section: | 10H-1 | 10H-2 |
|---|---|---|
| Interval (cm): | 148–150 | 0–2 |
| Layer: | AC* | AC* |
| Type: | AL | AL |
| N: | 14 | 15 |
| $SiO_2$ | 71.08 (0.49) | 71.49 (0.43) |
| $TiO_2$ | 0.17 (0.04) | 0.14 (0.04) |
| $Al_2O_3$ | 12.24 (0.19) | 12.18 (0.12) |
| FeO* | 2.28 (0.15) | 2.23 (0.14) |
| MnO | 0.08 (0.05) | 0.09 (0.05) |
| MgO | 0.01 (0.01) | 0.01 (0.01) |
| CaO | 1.14 (0.07) | 1.11 (0.04) |
| $Na_2O$ | 5.44 (0.29) | 5.36 (0.16) |
| $K_2O$ | 2.41 (0.13) | 2.38 (0.09) |
| Total | 94.85 | 94.99 |
| Q | 28.60 | 29.56 |
| Or | 14.94 | 14.73 |
| Ab | 48.30 | 47.53 |
| An | 1.96 | 2.26 |
| Ne | | |
| Di | 3.54 | 3.13 |
| Hy | 1.26 | 1.47 |
| Ol | | |
| Mt | 1.01 | 0.99 |
| Il | 0.34 | 0.28 |
| Total | 99.95 | 99.95 |

Notes: DA = dispersed ash; AL = ash layer. N = number of analyses. * = ash layer sampled at two depth intervals. Numbers in parentheses are one standard deviation of the mean. FeO* = total iron as FeO. C.I.P.W. norms calculated on water-free basis with 15% total iron as $Fe_2O_3$ and 85% as FeO.

**Table 3. Electron microprobe analyses and normative composition of basic and intermediate glassy tephra from Hole 907A.**

| Core, section: | 2H-3 | 2H-6 | 2H-6 | 5H-4 | 7H-5 | 7H-6 | 8H-3 | 8H-4 | 8H-6 | 9H-3 | 9H-3 |
|---|---|---|---|---|---|---|---|---|---|---|---|
| Interval (cm): | 118–119 | 139–141 | 139–141 | 36–38 | 90–92 | 120–122 | 97–98 | 39–41 | 120–122 | 35–37 | 35–37 |
| Layer: | F | G | G | K | P | Q | T | U | V | X | X |
| Type: | DA | AL | AL | AL | AL | AL | DA | AL | AL | AL | AL |
| N: | 10 | 12 | 2 | 15 | 10 | 9 | 14 | 16 | 13 | 13 | 2 |
| $SiO_2$ | 55.29 (1.78) | 51.31 (1.35) | 56.54 (0.49) | 52.53 (1.61) | 50.13 (0.51) | 51.86 (0.71) | 51.52 (0.76) | 51.63 (0.58) | 49.62 (0.34) | 49.67 (0.35) | 49.42 (0.00) |
| $TiO_2$ | 1.65 (0.23) | 3.24 (0.14) | 2.17 (0.00) | 3.10 (0.30) | 2.22 (0.20) | 1.12 (0.15) | 1.37 (0.09) | 1.79 (0.20) | 2.80 (0.13) | 2.54 (0.08) | 3.74 (0.22) |
| $Al_2O_3$ | 14.73 (0.24) | 12.74 (0.21) | 12.88 (0.28) | 13.41 (0.24) | 13.76 (0.24) | 16.25(1.47) | 14.65 (0.16) | 14.49 (0.37) | 13.85 (0.38) | 13.70 (0.16) | 13.45 (0.17) |
| FeO* | 11.17 (0.63) | 14.29 (0.35) | 12.78 (0.31) | 12.98 (0.71) | 12.53 (0.58) | 9.02 (0.92) | 11.06 (0.22) | 12.04 (0.57) | 14.01 (0.56) | 13.85 (0.28) | 14.93 (0.09) |
| MnO | 0.17 (0.06) | 0.25 (0.08) | 0.27 (0.05) | 0.27 (0.06) | 0.24 (0.03) | 0.17 (0.06) | 0.20 (0.05) | 0.22 (0.04) | 0.21 (0.04) | 0.22 (0.06) | 0.25 (0.03) |
| MgO | 3.92 (0.95) | 3.97 (0.16) | 2.23 (0.03) | 3.61 (0.32) | 5.84 (0.43) | 6.81 (0.74) | 6.52 (0.26) | 5.23 (0.53) | 6.07 (0.57) | 6.08 (0.17) | 5.03 (0.30) |
| CaO | 8.33 (1.15) | 8.31 (0.24) | 6.53 (0.14) | 7.80 (0.47) | 10.13 (0.47) | 12.92 (0.49) | 11.57 (0.28) | 10.18 (0.68) | 10.87 (0.44) | 11.39 (0.21) | 9.85 (0.09) |
| $Na_2O$ | 3.16 (0.22) | 2.91 (0.31) | 3.29 (0.12) | 3.70 (0.28) | 3.35 (0.45) | 2.49 (0.40) | 2.45 (0.14) | 2.83 (0.23) | 2.70 (0.28) | 2.59 (0.15) | 3.03 (0.12) |
| $K_2O$ | 0.76 (0.15) | 0.79 (0.05) | 1.24 (0.10) | 1.00 (0.14) | 0.59 (0.07) | 0.48 (0.15) | 0.62 (0.04) | 0.97 (0.13) | 0.37 (0.06) | 0.28 (0.04) | 0.65 (0.07) |
| $P_2O_5$ | 0.45 (0.13) | 0.65 (0.09) | 0.86 (0.08) | 1.31 (0.17) | 0.56 (0.03) | 0.35 (0.06) | 0.33 (0.04) | 0.41 (0.04) | 0.43 (0.04) | 0.42 (0.02) | 0.55 (0.03) |
| Total | 99.63 | 98.46 | 98.79 | 99.71 | 99.35 | 101.47 | 100.29 | 99.79 | 100.93 | 100.74 | 100.90 |
| Q | 8.80 | 6.61 | 13.33 | 5.59 | | 0.29 | 1.38 | 1.84 | 0.36 | 0.62 | 0.80 |
| Or | 4.42 | 4.63 | 7.26 | 5.80 | 3.44 | 2.75 | 3.59 | 5.63 | 2.12 | 1.61 | 3.71 |
| Ab | 26.34 | 24.42 | 27.59 | 30.73 | 27.94 | 20.46 | 20.30 | 23.52 | 22.13 | 21.27 | 24.80 |
| An | 23.42 | 19.22 | 16.57 | 16.73 | 20.48 | 30.83 | 26.59 | 23.56 | 23.81 | 24.20 | 20.50 |
| Di | 12.04 | 14.66 | 8.52 | 10.80 | 21.07 | 23.84 | 22.64 | 19.45 | 21.28 | 23.18 | 19.41 |
| Hy | 16.16 | 16.84 | 15.29 | 16.17 | 13.23 | 15.24 | 17.61 | 16.69 | 18.42 | 17.79 | 16.53 |
| Ol | | | | | 3.16 | | | | | | |
| Mt | 4.64 | 5.97 | 5.34 | 5.37 | 5.21 | 3.69 | 4.56 | 4.99 | 5.72 | 5.67 | 6.09 |
| Il | 3.10 | 6.12 | 4.09 | 5.79 | 4.17 | 2.07 | 2.55 | 3.35 | 5.16 | 4.69 | 6.89 |
| Ap | 0.97 | 1.41 | 1.86 | 2.81 | 1.21 | 0.74 | 0.71 | 0.88 | 0.91 | 0.89 | 1.16 |
| Total | 99.90 | 99.89 | 99.86 | 99.79 | 99.90 | 99.91 | 99.92 | 99.91 | 99.91 | 99.92 | 99.90 |

| Core, section: | 9H-6 | 10H-1 |
|---|---|---|
| Interval (cm): | 64–66 | 148–150 |
| Label: | Z | AC |
| Type: | AL | AL |
| N: | 13 | 15 |
| $SiO_2$ | 51.79 (1.98) | 48.88 (0.37) |
| $TiO_2$ | 3.45 (0.53) | 3.14 (0.12) |
| $Al_2O_3$ | 13.62 (0.26) | 13.26 (0.16) |
| FeO* | 13.75 (0.98) | 15.20 (0.22) |
| MnO | 0.23 (0.06) | 0.23 (0.05) |
| MgO | 4.09 (0.62) | 5.45 (0.12) |
| CaO | 8.28 (0.75) | 10.30 (0.16) |
| $Na_2O$ | 3.38 (0.50) | 2.71 (0.09) |
| $K_2O$ | 0.94 (0.18) | 0.44 (0.03) |
| $P_2O_5$ | 0.69 (0.22) | 0.46 (0.04) |
| Total | 100.22 | 100.07 |
| Q | 4.18 | 0.77 |
| Or | 5.42 | 2.53 |
| Ab | 27.90 | 22.35 |
| An | 18.76 | 22.16 |
| Di | 14.16 | 20.61 |
| Hy | 15.92 | 18.44 |
| Ol | | |
| Mt | 5.65 | 6.25 |
| Il | 6.41 | 5.83 |
| Ap | 1.47 | 0.98 |
| Total | 99.88 | 99.91 |

Notes: DA = dispersed ash, AL = ash layer. N = number of analyses. Numbers in parentheses are one standard deviation of the mean. FeO* = total iron as FeO. C.I.P.W. norms calculated on water-free basis with 15% total iron as $Fe_2O_3$ and 85% as FeO.

in the late Pliocene layer Q as well (Fig. 6). Large compositional ranges characterize glass of basaltic andesitic affinity, with MgO values ranging from 5.5 to 2 wt% for the Pleistocene layers A, B, F, G; between about 7.5 and 5 wt% for the late Pliocene layer Q; and between about 8.5 and 5.5 wt% for the early Pliocene layer V (Figs. 5–7). The extensive chemical heterogeneity observed in the Pleistocene horizons A, B, and F is interpreted to be related to their occurrence as dispersed ash of multiple sources (i.e., ash zones) (Table 1).

The $TiO_2$ vs. $K_2O$ plot is a useful tool to discriminate between alkalic and sub-alkalic basalts and basaltic andesites derived from Iceland and other North Atlantic sources (Jakobsson, 1979b; Larsen, 1981; Lacasse et al., 1995). Figure 8 shows FeO*/$TiO_2$ fields of basic tephra recovered at Site 907 for the Pleistocene, and the late and early Pliocene periods. Data for postglacial basalts from six volcanic systems on the Eastern Volcanic Zone (Veidivötn, Vestmannaeyjar, Grímsvötn, Vatnafjöll, Hekla, and Katla) were compiled by Jakobsson (1979b) and show characteristic compositional fields (Fig. 8). Average compositions of dredged basaltic glasses from the Mid-Atlantic Ridge (MAR) are presented in Sigurdsson (1981) and are also shown in Figure 8 for five different Mg-value ranges. Analyses of glasses (Group A after Sigurdsson, 1981) from the MAR segment between the Gibbs Fracture Zone (from 54°N) along the Reykjanes Ridge and the Kolbeinsey Ridge (up to 70°N) exhibit MgO concentrations ranging from 9.3 to 6.1 wt%, with Mg-values from 46 to 66. The glasses are characterized by low K content; $K_2O$ ranges from 0.04 to 0.11 wt%. $TiO_2$ content of the same glasses varies between 1.02 and 1.66 wt% (Fig. 8). Analyses of basaltic glass from the Kolbeinsey Ridge indicate the same compositional ranges (Lackschewitz and Wallrabe-Adams, 1991; Lackschewitz et al., 1994).

None of the basic tephra of Site 907 have chemical compositions similar to typical MAR basalts. All the basaltic components of the ash layers have $K_2O$ concentration higher than 0.2 wt%, which is the

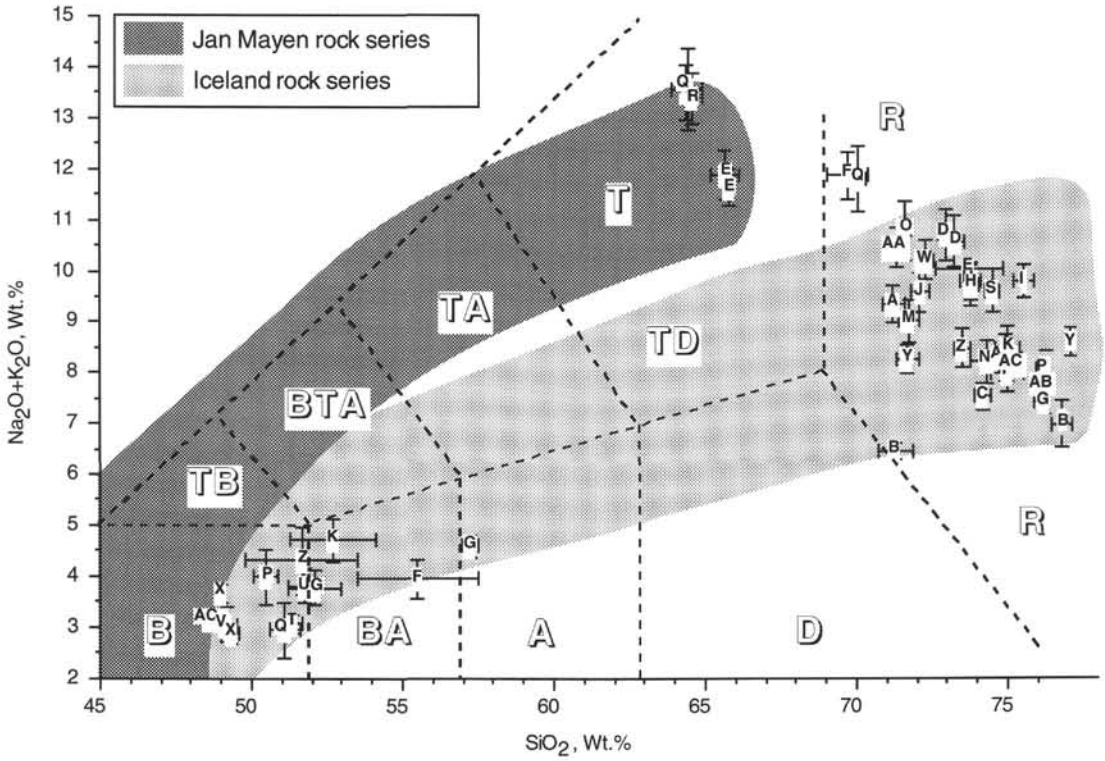


Figure 4. Total alkali–silica (TAS) plot indicating classification (after Le Bas et al., 1986), on an anhydrous basis, of glass shards (mean and standard deviation) from Site 907, Iceland Plateau. Fields are B = basalt, BA = basaltic andesite, A = andesite, D = dacite, R = rhyolite, TD = trachydacite, T = trachyte, TA = trachyandesite, BTA = basaltic trachyandesite, and TB = trachybasalt. All analyses have been normalized to a total of 100%. Fields for Jan Mayen and Iceland Holocene and upper Pleistocene rock suites (whole-rock compositions) are from Imsland (1984) and Jakobsson (1979a), respectively.

maximum value for basaltic glass from the MAR segment between 54°N and 70°N. Except for layers X, V, and AC, the potential sources for the basic tephra are thus located in Iceland, because these layers plot outside of the TAS field for the Jan Mayen rock suite (Fig. 4). Judging from Figure 8, the Eastern Volcanic Zone in Iceland may have been the source of these tephra. Other volcanic zones in Iceland, active at that time, have to be considered also (Sigurdsson et al., 1978; Meyer et al., 1985).

TAS plots of the majority of rhyolitic and trachytic tephra of Site 907 indicate a very homogeneous glass composition (Fig. 4). This chemical characteristic of silicic tephra makes them generally more useful than their basic counterparts as chronostratigraphic markers in marine sediments and ice cores. They can be easily identified and correlated to sources on land (Lacasse et al., 1995, 1996, in press). Figure 4 shows that most of the rhyolitic tephra have an Icelandic affinity, and that the trachytic tephra (layers E, Q, and R) were likely derived from the Jan Mayen region.

## Silicic Glass

The silicic tephra of Site 907 can be divided into compositional classes from their chemical composition (Table 2), using potassium as the principal discriminant (Sigurdsson and Loebner, 1981). It subdivides the trachytic and rhyolitic compositions into a high-potassium and a low-potassium series. These two series were also discriminated on the basis of other elements, such as FeO* and CaO. Silicic glass analyses from Site 907 were compared for the Pleistocene, and the late and early Pliocene (Figs. 9–11). According to the Sigurdsson and Loebner (1981) water-free compositional classification (table 1, p. 302), rhyolite tephra ($K_2O < 3.8$ wt%, $2 < FeO^* < 6.5$ wt% and $1 < CaO < 3$ wt%) were produced during the three periods with layers A, B, C, G, J for the Pleistocene; layers K, L, M, N, and P for the late Pliocene; and layers Y, Z, AB, and AC for the early Pliocene. Tephra of alkali rhyolite composition ($K_2O > 3.8$ wt%, $1 < FeO^* < 5$ wt%, $CaO < 1.7$ wt%) occur as layers E, F, and I; layers O, Q, R, and S; and layers Y and AA for the same three geological intervals. A third type of rhyolitic glass with low alumina and calcium contents ($Al_2O_3 < 11.2$ wt% and $CaO < 0.25$ wt%; i.e., peralkaline rhyolite or comendite) was found in layers D and I (Pleistocene). Layer Q (late Pliocene) and layer W (early Pliocene) show affinity close to the comenditic type with slightly higher calcium content.

Normative salic components (quartz, albite, anorthite, orthoclase, etc.) of the rhyolitic tephra of Site 907 make up between 68 (layer Q) and 97 wt% (layer Y) of the glasses (Table 2). When plotted in the granite system Ab-Or-$SiO_2$ (Thompson and MacKenzie, 1967; Sigurdsson, 1971), all the rhyolitic glasses fall within the plagioclase volume for water pressures less than 1 kilobar (Fig. 12). The three rhyolitic glass types described above define distinct fields on either side of the boundary between the low-K and high-K groups of Sigurdsson and Loebner (1981). The rhyolitic tephra plot on the albite side and the alkali-rhyolitic on the orthoclase side of this boundary. Compositional differences between the two series are more likely due to difference in the original bulk source rock composition and the extent of melting. High-K rhyolitic melts coexisted with alkali feldspar, quartz, and with or without plagioclase, and low-K rhyolitic melts coexisted with plagioclase alone and pyroxene (Fig. 12). Peralkaline rhyolitic compositions in layers D, I, and Q represent a separate group, which plots close to or on the minimum melting temperature curve for water pressure of 1 kb, and for approximately equal amounts of normative quartz, albite, and orthoclase (Fig. 12).

Site 907 tephra of trachytic composition can be divided into two subgroups: Qz-normative (layer E with Qz = 4.72–6.12 wt%) and

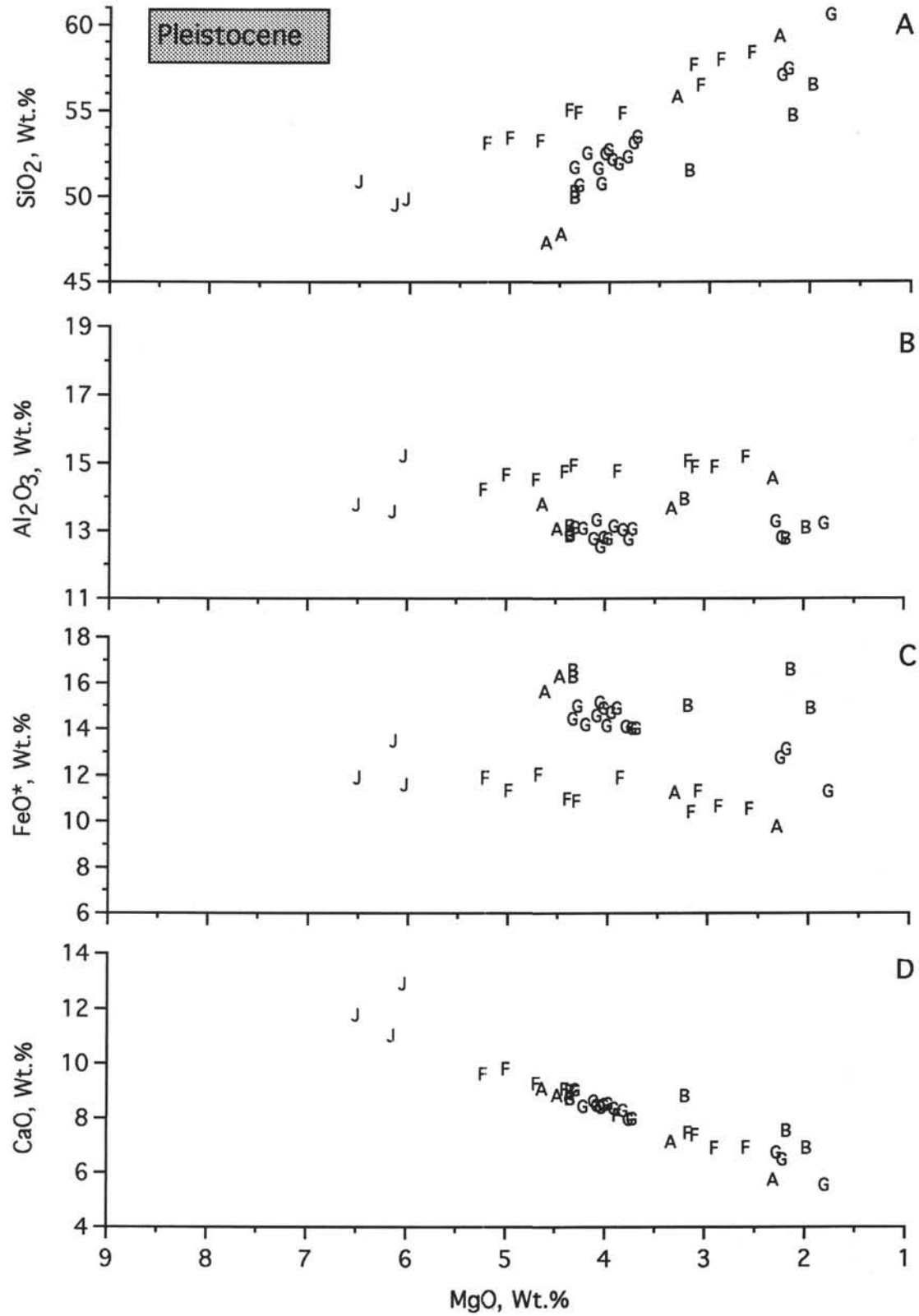


Figure 5. Fields of basaltic and basaltic andesitic glasses from Pleistocene tephra in Hole 907A in (**A**) $SiO_2$/MgO, (**B**) $Al_2O_3$/MgO, (**C**) FeO*/MgO, and (**D**) CaO/MgO diagrams. Plots are vs. decreasing MgO concentration. All analyses have been normalized to a total of 100%.

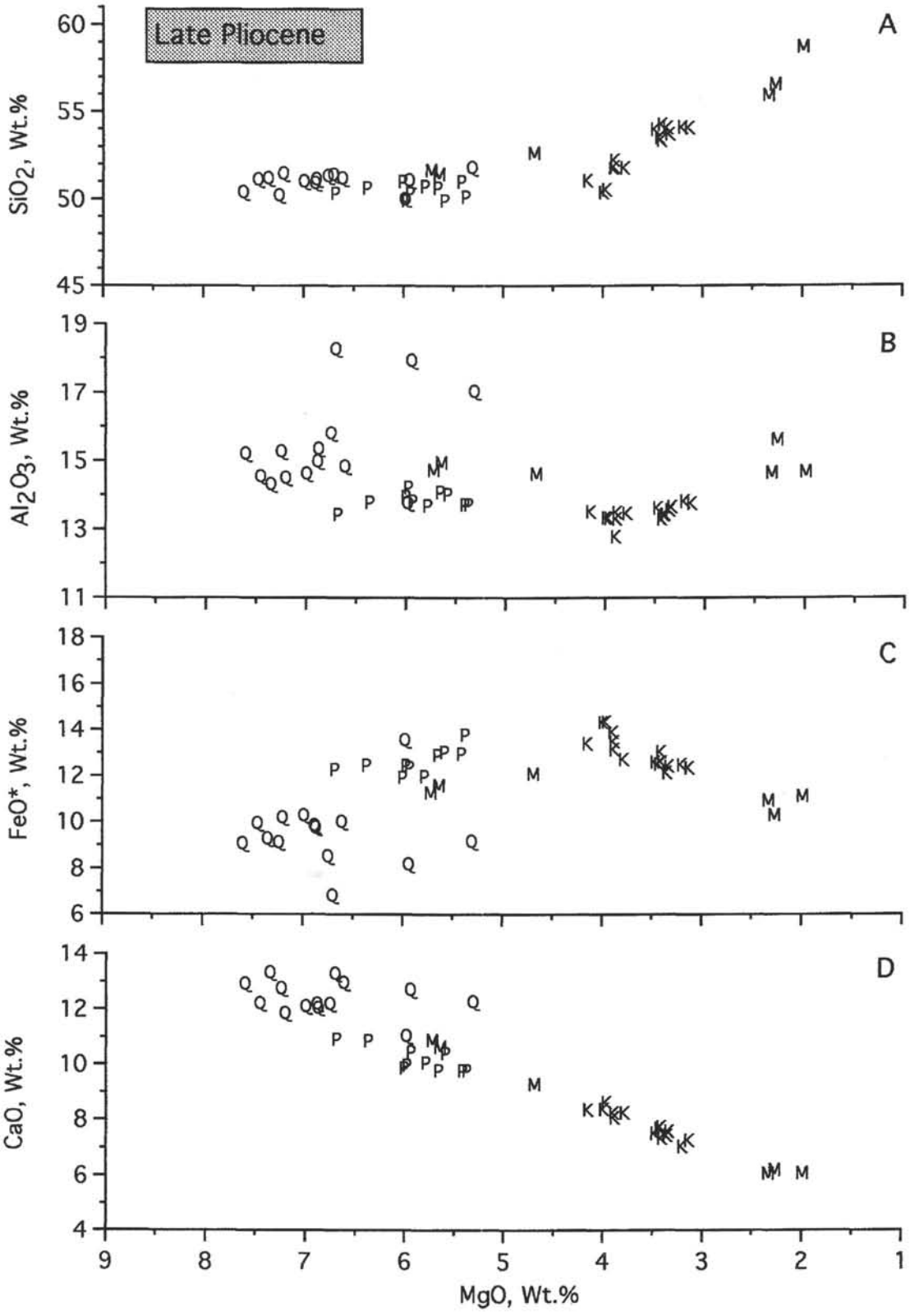


Figure 6. Fields of basaltic and basaltic andesitic glasses from late Pliocene tephra in Hole 907A in (**A**) $SiO_2$/MgO, (**B**) $Al_2O_3$/MgO, (**C**) FeO*/MgO, and (**D**) CaO/MgO diagrams. Plots are vs. decreasing MgO concentration. All analyses have been normalized to a total of 100%.

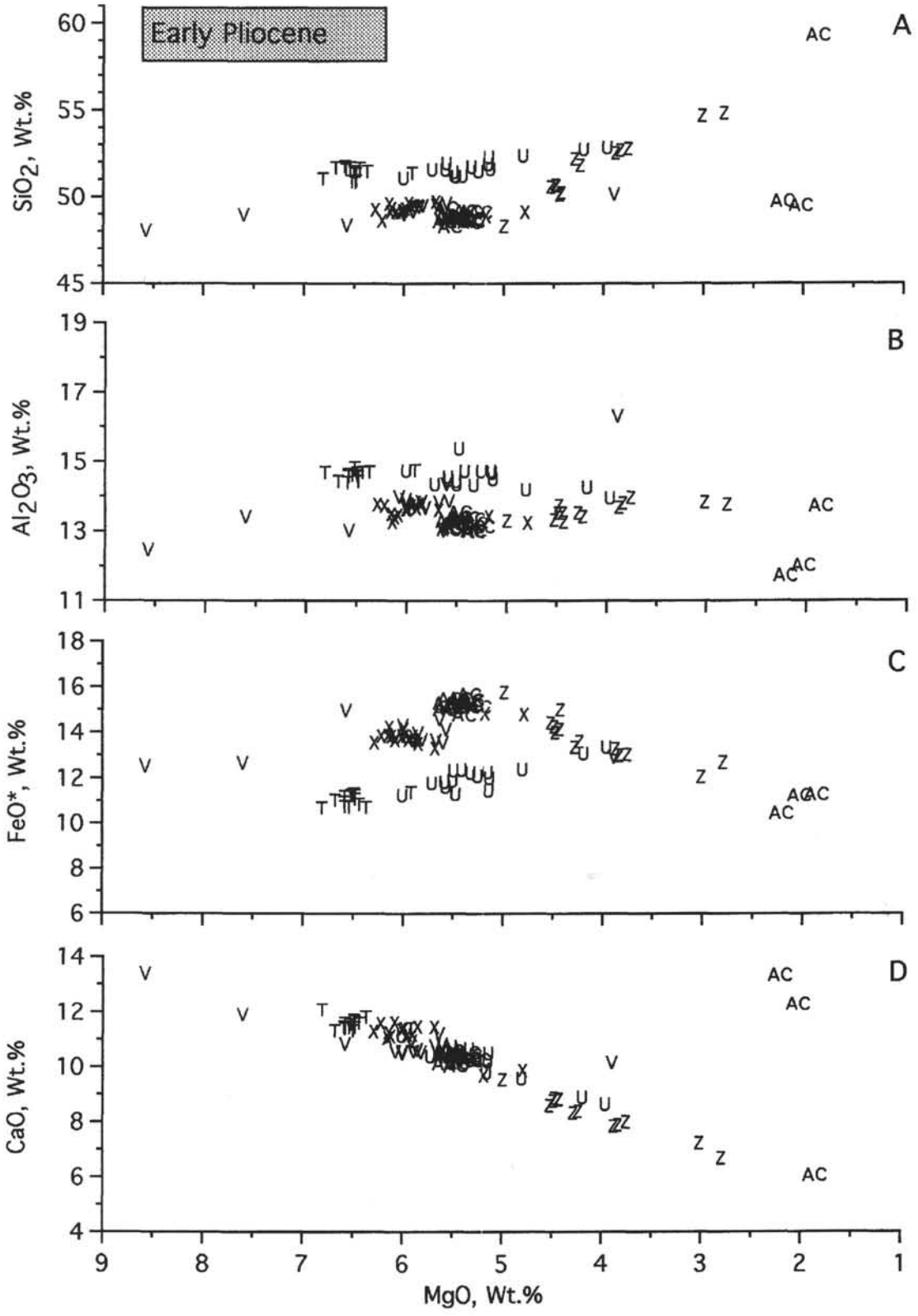


Figure 7. Fields of basaltic and basaltic andesitic glasses from early Pliocene tephra in Hole 907A in (**A**) $SiO_2$/MgO, (**B**) $Al_2O_3$/MgO, (**C**) FeO*/MgO, and (**D**) CaO/MgO diagrams. Plots are vs. decreasing MgO concentration. All analyses have been normalized to a total of 100%.

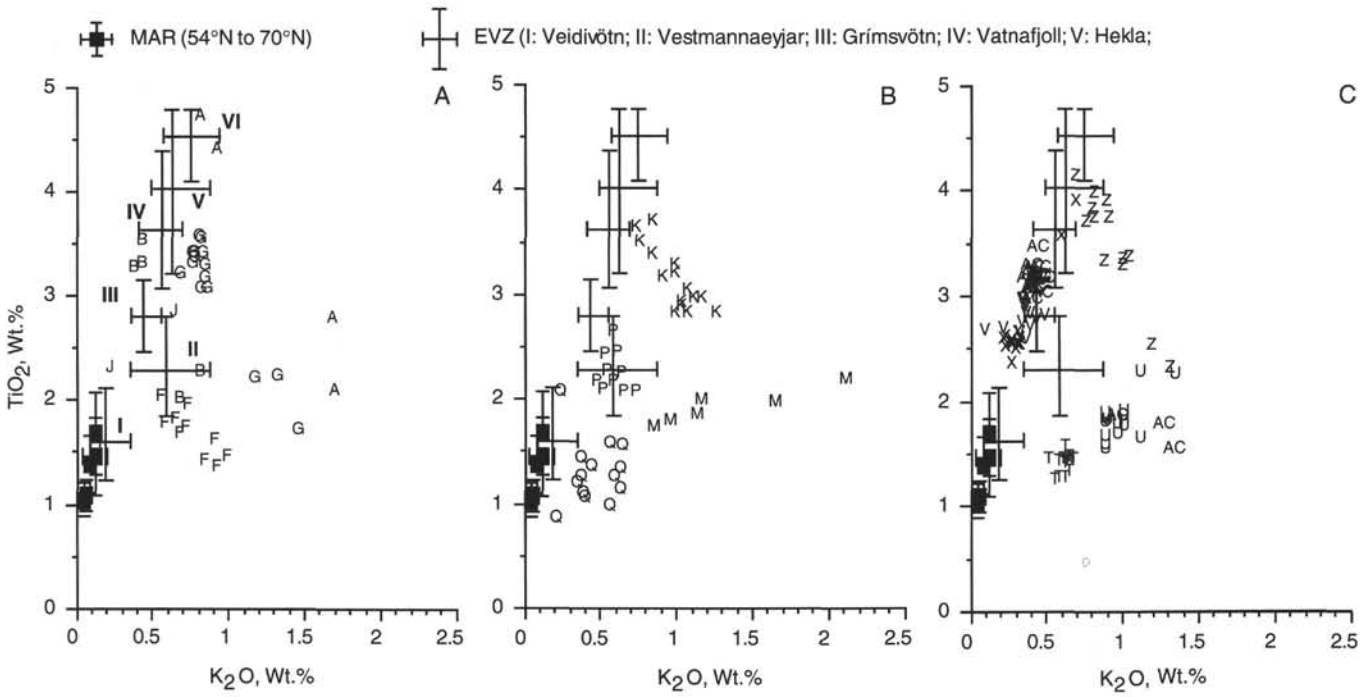


Figure 8. $TiO_2/K_2O$ plots for basaltic and basaltic andesitic glasses from (**A**) Pleistocene, (**B**) late Pliocene, and (**C**) early Pliocene tephra in Hole 907A. All analyses have been normalized to a total of 100%. Fields for the Eastern Volcanic Zone (EVZ) in Iceland after Jakobsson (1979b). Fields for the Mid-Atlantic Ridge (MAR) after Sigurdsson (1981).

Ne-normative (layers R and Q with Ne = 1.35–1.94 wt%) (Table 2). Qz-trachytic tephra E was erupted during the Pleistocene, whereas the two Ne-trachytic tephra Q and R are dated of late Pliocene age (Figs. 9, 10). Both trachytic compositions are characterized by high potassium and high alumina contents ($K_2O > 5$ wt% and $Al_2O_3 > 16$ wt%). Ne-normative trachytic glass is more sodic, with $Na_2O$ exceeding 7 wt% (layers Q and R) and less calcic than the Qz-normative trachytes (layer E). The Jan Mayen volcanic system is known to have produced trachybasaltic rock series during at least the Pleistocene and may be considered the most likely source for tephra of trachytic composition recovered on the Iceland Plateau. Analysis of matrix glass of trachytic pumices from the alkalic volcano Snæfellsjökull (tephra Sn3; Jóhannesson et al., 1981) in western Iceland indicates in comparison a lower total alkali content of about 9.9 wt%, or less than the alkali content of trachytic tephra (layers E, Q, and R) from Site 907.

### Trace Elements

Trace element data of bulk ash layers are presented in Table 4. Only crystal-poor ash layers with less than 10% crystals were analyzed for trace elements. Chondrite-normalized REE spectra were used to compare the patterns of the Pliocene and Pleistocene ash layers of Site 907 with those characteristic of the Iceland and Jan Mayen rock series (Oskarsson et al., 1982; Maaløe et al., 1986) (Fig. 13). REE concentrations were normalized in both cases to the mean chondritic C1 composition of Anders and Grevesse (1989). REE patterns in Figure 13A–C reflect the LREE-enriched character of the tephra samples and the enrichment in REE with increasing silica content. The REE patterns for the homogeneous rhyolitic tephra C, D, H, I, L, N, S, W, Y, Z, AB show a pronounced negative Eu anomaly, indicative of varying amount of plagioclase in equilibrium with the parental magma. Heavy-REE concentrations of 10 times chondritic suggest that garnet was absent from the source (Fig. 13). The comparison of the REE pattern of rhyolitic tephra from Site 907 with the REE-spectra of volcanics from Iceland supports their origin from this volcanic source and unlikely from the trachybasaltic suite of Jan Mayen (Fig. 13D). REE patterns for the homogeneous basaltic layers U, X, and Z show the lowest light-REE enrichment incompatible also with a Jan Mayen source (Fig. 13C–D). In contrast, chondrite-normalized REE spectra for the trachytic layers E and R show a very specific pattern almost identical to that of a Jan Mayen counterpart (anal. 15 after Maaløe et al., 1986), bringing little doubt as to their origin. In both cases they are characterized by high light-REE enrichment with a pronounced negative slope, while the heavy-REE segment is almost flat, with a concentration factor of about 20 times chondritic (Fig. 13A, B, D).

## DISCUSSION

From the temporal distribution of ash layers at Site 907 (Fig. 2) we can infer several episodes of more frequent tephra deposition on the Iceland Plateau, which may be indication of more intense volcanism in the region. Two major periods of more frequent ash deposition occurred at the beginning of the early Pliocene, between about 5.5 and 5.0 Ma, and the beginning of the late Pliocene, between about 3.5 and 3.0 Ma. These periods are characterized by the deposition of either bimodal or silicic tephra, generated by large explosive eruptions. They are separated by a period of approximately 1.5 m.y. of deposition of essentially basaltic or basaltic andesite tephra, with the exception of one rhyolitic ash layer.

Interpretation of the frequency of ash layer occurrence for the last 3 m.y. (i.e., the Pliocene–Pleistocene and upper Pleistocene) is complicated by the influence of glaciation in the region. Only two tephra layers have been found that date between 3.0 and 1.5 Ma at Site 907 (Fig. 2). The middle and upper Pleistocene is characterized by the relatively steady deposition of ash layers and ash zones, but with a pe-

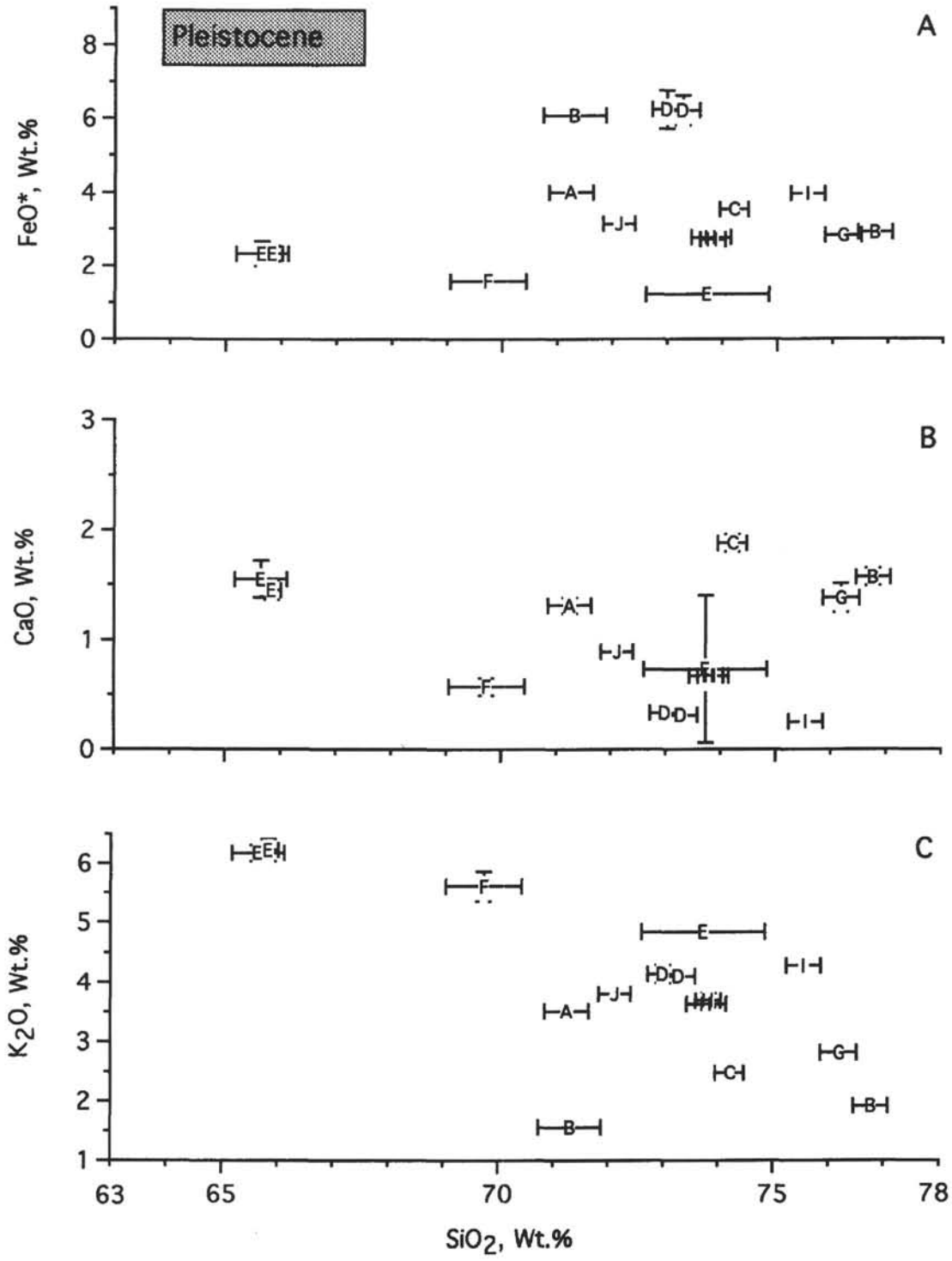


Figure 9. Fields of trachytic and rhyolitic glasses from Pleistocene tephra in Hole 907A in (**A**) FeO*/$SiO_2$, (**B**) CaO/$SiO_2$, and (**C**) $K_2O$/$SiO_2$ diagrams. All analyses have been normalized to a total of 100%. Crosses are mean and standard deviation.

riod between isotope Stages 15 and 8 (620–245 ka) where the sediment is devoid of ash deposition. All the Pleistocene ash layers and ash zones are either bimodal in composition or silicic. No pure basaltic ash layers have been found for this interval.

The land masses adjacent to the Iceland Plateau are known to have undergone episodic glaciations, which date back as early as 5.45 Ma (Jansen et al., 1990). The recovery of dropstones from about 6.5 Ma at Site 907 suggests even older episodes, related to the onset of ice-sheets on the adjacent continents (Leg 151 Shipboard Scientific Party, 1995). Therefore, we can assume that all the Pliocene and Pleistocene ash layers of Site 907 were deposited in a marine environment influenced by repeated episodes of growth and decay of continental ice-sheets as well as of sea-ice cover, which reached their full amplitude during the late Pleistocene. It is likely that fluctuation of sea-ice

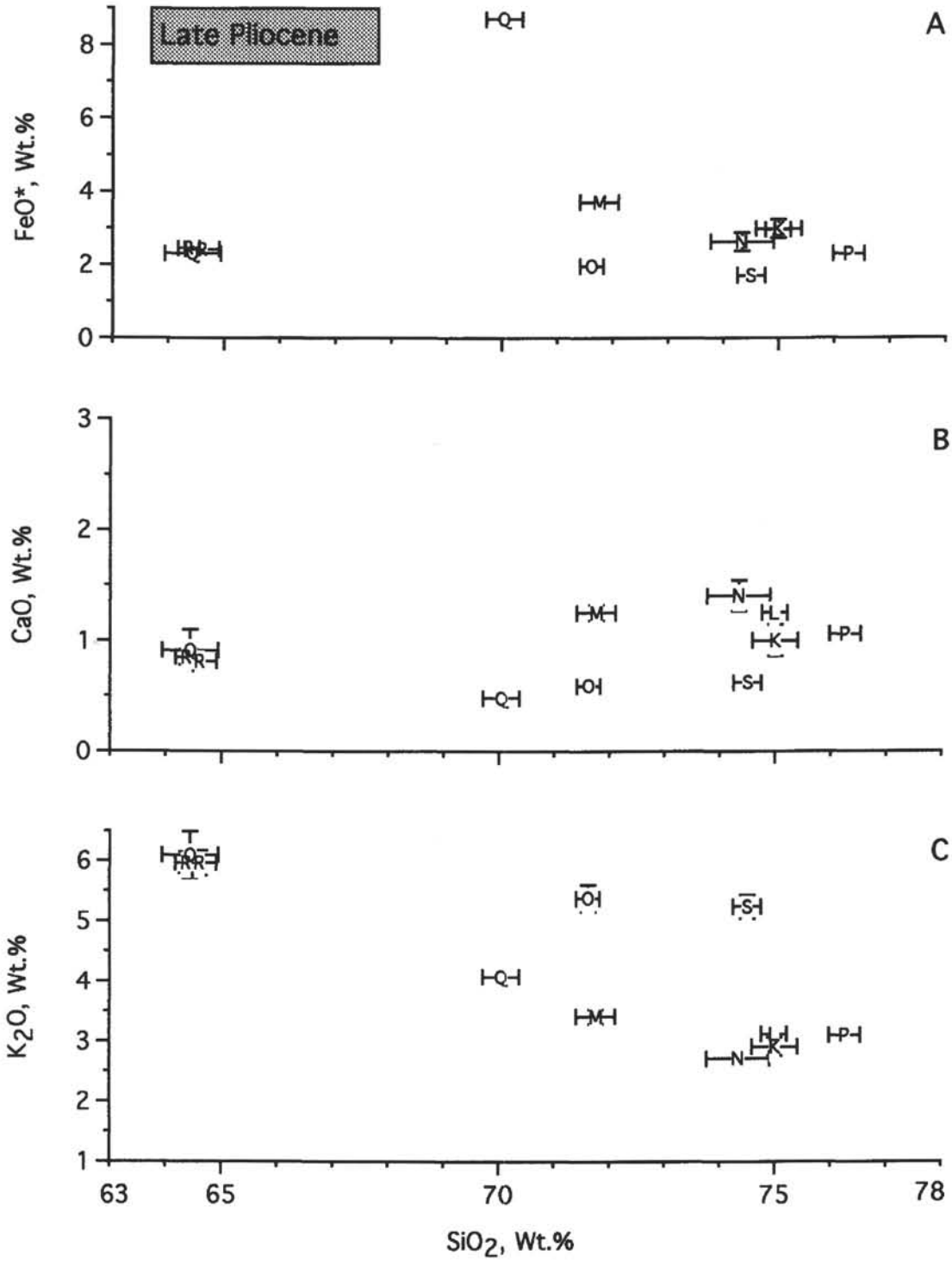


Figure 10. Fields of trachytic and rhyolitic glasses from late Pliocene tephra in Hole 907A in (**A**) $FeO^*/SiO_2$, (**B**) $CaO/SiO_2$, and (**C**) $K_2O/SiO_2$. All analyses have been normalized to a total of 100%. Crosses are mean and standard deviation.

distribution north of Iceland complicated the deposition of ash fallout from Iceland or Jan Mayen. At the present time (interglacial), the distribution and density of sea ice in the area is seasonal (Wells et al., 1995). The sea-ice extent in the polar and subpolar region of the North Atlantic during the Last Glacial Maximum (LGM, 18 ka) was reconstructed by Kellogg (1980). The permanent and seasonal sea-ice cover was much greater than present and likely prevented the direct deposition of ash layers north of Iceland (fig. 18 in Lacasse et al., 1996. None of the ash layers or ash zones found in upper Pleistocene sediments of Site 907 can be correlated to Ash Zone 2 in the North Atlantic. This marine tephra is known to have been generated from an Icelandic volcano, at approximately 55 ka, during glacial condi-

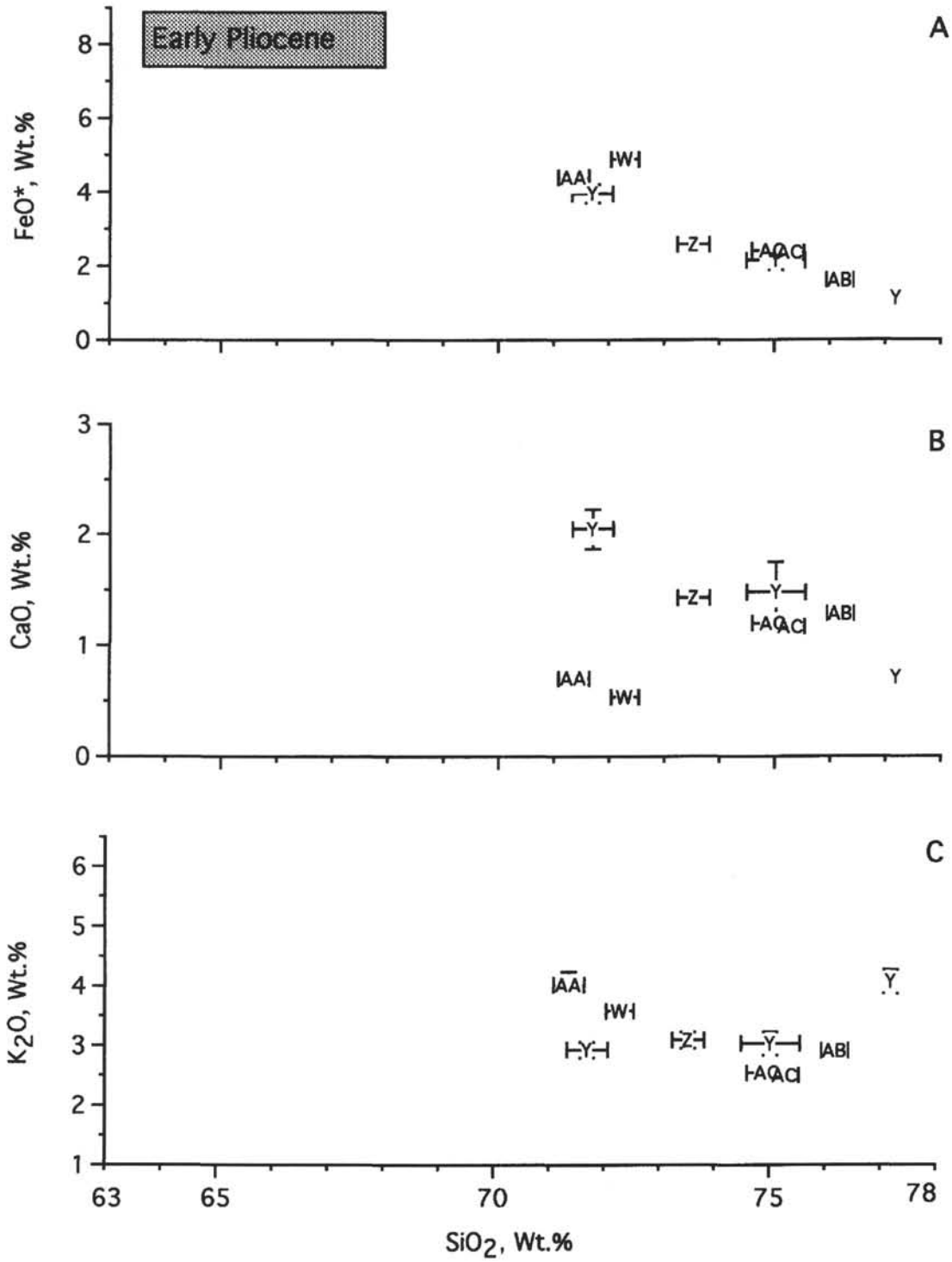


Figure 11. Fields of rhyolitic glasses from early Pliocene tephra in Hole 907A in (**A**) FeO*/$SiO_2$, (**B**) CaO/$SiO_2$, and (**C**) $K_2O$/$SiO_2$ diagrams. All analyses have been normalized to a total of 100%. Crosses are mean and standard deviation.

tions similar to the LGM (Lacasse et al., 1996). The absence of the same ash zone in Core P57–7 (Sejrup et al., 1989; Sjøholm et al., 1991), located about 100 km south-southwest of ODP Site 907 (Fig. 1), indicates that its deep-sea deposition as subaerial fallout was likely prevented by the presence of dense sea-ice covering the southern Norwegian Sea at that time.

In contrast, four major ash zones were found occurring in Core P57-7 (Fig. 1), during interglacial Stages 1, 5e, 7, and 9 (Sejrup et al., 1989; Sjøholm et al., 1991). The recovery of layers A (Stage 1), B (Stage 5e), and C and D (Stage 7) at Site 907 confirms this observation (Fig. 2). The uppermost ash zone in both Core P57-7 and Core 151-907A-1H was correlated to Ash Zone 1, 11–11.1 ka, after Bard

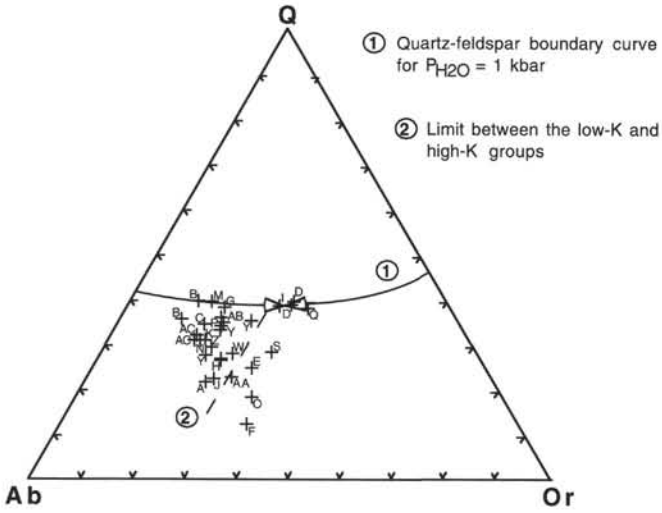


Figure 12. Normative projection of rhyolitic tephra from Site 907 in the "granite" system. The quartz-feldspar boundary curve is for $P_{H2O}$ = 1 kb (after Thompson and MacKenzie, 1967; Sigurdsson, 1971). The dashed line indicates the limit between the low-K and high-K groups (after Sigurdsson and Loebner, 1981).

et al. (1994), based on both chemical and stratigraphic evidence. Correlation of the other tephra layers between the two coring sites on the Iceland Plateau is suggested by their stratigraphic position rather than by their major element chemistry. Analytical problems of Na loss and silica gain for the rhyolitic tephra of Core P57-7 (Sjøholm et al., 1991) make it difficult to do any reliable chemical correlation with their counterparts in cores from Hole 907A.

Sejrup et al. (1989) concluded that the distribution of upper Pleistocene ashes in Core P57-7 on the Iceland Plateau was not primarily controlled by sea-ice and atmospheric conditions but by an increase in the volcanic activity on Iceland during interglacial (light isotopic) stages. Assuming unchanged atmospheric circulation, they inferred that explosive eruptions of magnitude larger than the normal Holocene eruptions took place in the late Pleistocene, as a result of pressure release on magma chambers due to major deglaciations of the Iceland ice cap. However, thickness and grain-size characteristics of lower Pliocene ash layers at Site 907 (Table 1; Fig. 3) show that they were also produced by Icelandic eruptions of at least the same magnitude, during a period when Iceland was not covered by an ice cap. According to Geirsdóttir and Eiríksson (1994), the first signs of local glaciation appeared in southeastern Iceland between 4.0 and 3.0 Ma, and a more extensive glaciation from 2.4 to 2.5 Ma. Since this time Iceland has been subject to full-scale glacial-interglacial cyclicity with an ice sheet covering most of the island. Based on this constraint it appears difficult to simply relate the magnitude of pre-Holocene Iceland eruptions to climate forcing. The record more likely represents a combination of factors, including (1) pressure changes due to glacial loading/unloading, (2) variations in tectonic/rifting activity, (3) changes in paleowind circulation associated with glacial/interglacial cycles. Furthermore, the production of the widespread ice-rafted Ash Zone 2 in the North Atlantic, during the early stages of the last glaciation, shows that large explosive eruptions in Iceland also occur during a glacial period (Lacasse et al., 1995, 1996).

## CONCLUSIONS

Major and trace element chemistry of the Pliocene and Pleistocene ash layers of Site 907 indicates that Iceland and, to a lesser extent, Jan Mayen were the two major volcanic sources supplying tephra to the Iceland Plateau. Compositionally bimodal (basaltic and rhyolitic) and rhyolitic ash layers have a chemical affinity with an Icelandic source. The majority show a dominant tholeiitic trend, from tholeiitic basalt to rhyolite, but with some intermediate compositions of basaltic andesite and icelandite, that are compatible with a source from the Pliocene and Pleistocene rift zones in Iceland. Some rhyolitic layers show an alkalic or peralkaline (comenditic) composition, indicative of a source from the only two regions in Iceland having produced alkali and transitional-alkali rock series during this period: the Snæfellsnes Peninsula and the Eastern Volcanic Zone.

In contrast, some marine tephra of trachytic composition show a total alkalinity (sodium and potassium content) incompatible with known sources in Iceland, even from its most alkalic volcanic centers. The most recent trachytic tephra was produced during the middle Pleistocene and was most likely associated with the trachy-basaltic rock series of Jan Mayen Island. However, the production of tephra of trachytic composition during the late Pliocene raises the question of the involvement of Jan Mayen itself, because its oldest exposed lavas are of upper Pleistocene (Sylvester, 1975), and consequently makes the continental Jan Mayen Ridge or the Eggvin Bank a possible source.

All of the homogeneous basaltic tephra exhibit glass compositions incompatible with an origin from the Kolbeinsey Ridge, between Iceland and the Jan Mayen Fracture Zone. Total alkali content suggest that they were likely derived from the tholeiitic rock series in Iceland.

Based on their sedimentological and grain-size characteristics, and location from source, the ash layers, with very few exceptions, were derived from tephra fallout from large explosive eruptions in Iceland and Jan Mayen, followed by settling and size fractionation through the water column.

## ACKNOWLEDGMENTS

We thank Joseph Devine for assistance with microprobe analyses at the Geological Sciences Department of Brown University. This research benefited greatly from information provided by Frank Rack (GRAPE-density and magnetic susceptibility measurements), Torben Fronval ($\delta^{18}O$ stratigraphy) and David Williamson (paleomagnetic stratigraphy). The authors express their sincere thanks to Leonard Johnson and two anonymous reviewers for their constructive reviews. Lacasse's work was supported by a grant from JOI/USSAC and is part of a Ph.D. dissertation.

## REFERENCES

Anders, E., and Grevesse, N., 1989. Abundances of the elements: meteoritic and solar. *Geochim. Cosmochim. Acta,* 53:197–214.

Bard, E., Arnold, M., Mangerud, J., Paterne, M., Labeyrie, L., Duprat, J., Mélières, M.-A., Sønstegaard, E., and Duplessy, J.-C., 1994. The North Atlantic atmosphere-sea surface $^{14}C$ gradient during the Younger Dryas climatic event. *Earth Planet. Sci. Lett.,* 126:275–287.

Bitschene, P.R., Schmincke, H.-U., and Viereck, L., 1989. Cenozoic ash layers on the Vøring Plateau (ODP Leg 104). *In* Eldholm, O., Thiede, J., Taylor, E., et al., *Proc. ODP, Sci. Results,* 104: College Station, TX (Ocean Drilling Program), 357–366.

Cande, S.C., and Kent, D.V., 1992. A new geomagnetic polarity time scale for the Late Cretaceous and Cenozoic. *J. Geophys. Res.,* 97:13917–13951.

CLIMAP Project Members, 1981. Seasonal reconstructions of the Earth's surface at the last glacial maximum. *Geol. Soc. Am., Map and Chart Ser.,* MC36.

Damuth, J.E., 1978. Echo character of the Norwegian-Greenland Sea: relationship to Quaternary sedimentation. *Mar. Geol.,* 28:1–36.

Desprairies, A., Maury, R.C., Joron, J.-L., Bohn, M., and Tremblay, P., 1989. Distribution, chemical characteristics, and origin of ash layers from ODP Leg 104, Vøring Plateau, North Atlantic. *In* Eldholm, O., Thiede, J., Tay-

lor, E., et al., *Proc. ODP, Sci. Results,* 104: College Station, TX (Ocean Drilling Program), 337–356.

Donn, W.L., and Ninkovich, D., 1980. Rate of Cenozoic explosive volcanism in the North Atlantic ocean inferred from deep-sea cores. *J. Geophys. Res.,* 85:5455–5460.

Eldholm, O., Thiede, J., Taylor, E., et al., 1987. *Proc. ODP, Init. Repts.,* 104: College Station, TX (Ocean Drilling Program).

Folk, R.L., 1974. *Petrology of Sedimentary Rocks*: Austin, TX (Hemphill Publ.).

Geirsdóttir, A., and Eiríksson, J., 1994. Growth of an intermittent ice sheet in Iceland during the late Pliocene and early Pleistocene. *Quat. Res.,* 42:115–130.

Imbrie, J., Hays, J.D., Martinson, D.G., McIntyre, A., Mix, A.C., Morley, J.J., Pisias, N.G., Prell, W.L., and Shackleton, N.J., 1984. The orbital theory of Pleistocene climate: support from a revised chronology of the marine $\delta^{18}O$ record. *In* Berger, A., Imbrie, J., Hays, J., Kukla, G., and Saltzman, B. (Eds.), *Milankovitch and Climate* (Pt. 1), NATO ASI Ser. C, Math Phys. Sci., 126: Dordrecht (D. Reidel), 269–305.

Imsland, P., 1984. Petrology, mineralogy and evolution of the Jan Mayen magma system. *Soc. Scient. Islandica,* 43.

INQUA Inter-Congress Committee on Tephrochronology, 1990. Standardisation of the chemical analysis of tephra deposits. *Field Conference and Workshop on Tephrochronology: Abstracts,* Mammoth Hot Springs, Yellowstone National Park, 55–60.

Jakobsson, S.P., 1979a. Outline of the petrology of Iceland. *Jokull,* 29:57–73.

————, 1979b. Petrology of recent basalts of the Eastern Volcanic Zone, Iceland. *Act. Naturalia Isl.,* 26.

Jansen, E., and Sjøholm, J., 1991. Reconstruction of glaciation over the past 6 Myr from ice-borne deposits in the Norwegian Sea. *Nature,* 349:600–603.

Jansen, E., Sjøholm, J., Bleil, U., and Erichsen, J.A., 1990. Neogene and Pleistocene glaciations in the northern hemisphere and late Miocene-Pliocene global ice volume fluctuations: evidence from the Norwegian Sea. *In* Bleil, U., and Thiede, J. (Eds.), *Geological History of the Polar Oceans: Arctic Versus Antarctic:* Dordrecht (Kluwer), 677–705.

Jóhannesson, H., Flores, R.M., and Jónsson, J., 1981. A short account of the Holocene tephrochronology of the Snæfellsjökull central volcano, western Iceland. *Jokull,* 31:23–30.

Johnson, G.L., 1974. Morphology of the Mid Ocean Ridge between Iceland and the Arctic. *In* Kristjansson, L. (Ed.), *Geodynamics of Iceland and the North Atlantic Area:* Dordrecht (D. Reidel), 49–62.

Johnson, G.L., Southall, I.R., Young, D.W., and Vogt, P.R., 1972. Origin and structure of the Iceland Plateau and Kolbeinsey Ridge. *J. Geophys. Res.,* 77:5688–5696.

Kellogg, T.B., 1973. Late Pleistocene climatic record in Norwegian and Greenland Sea deep-sea cores [Ph.D. thesis]. Columbia Univ., New York.

————, 1980. Paleoclimatology and paleo-oceanography of the Norwegian and Greenland Seas, glacial-interglacial contrasts. *Boreas,* 9:115–137.

Kutzbach, J.E., and Guetter, P.J., 1986. The influence of changing orbital parameters and surface boundary conditions on climate simulations for the past 18,000 years. *J. Atmos. Sci.,* 43:1726–1759.

Kutzbach, J.E., and Wright, H.E., 1985. Simulation of the climate of 18,000 years BP: results for the North American/North Atlantic/European sector and comparison with the geological record of North America. *Quat. Sci. Rev.,* 4:147–187.

Lacasse, C., Sigurdsson, H., Carey, S., Paterne, M., and Guichard, F., 1996. North Atlantic deep-sea sedimentation of Late Quaternary tephra from the Iceland hotspot. *Mar. Geol.,* 129:207–235.

Lacasse, C., Sigurdsson, H., Jóhannesson, H., Paterne, M., and Carey, S., 1995. Source of Ash Zone 1 in the North Atlantic. *Bull. Volcanol.,* 57:18–32.

Lacasse, C., Werner, R., Paterne, M., Sigurdsson, H., Carey, S., and Pinte, G., in press. Long-range transport of Icelandic tephra to the Irminger Basin, Site 919. *In* Saunders, A.D., Larsen, H.C., Clift, P.D., and Wise, S.W., Jr. (Eds.), *Proc. ODP, Sci. Results,* 152: College Station, TX (Ocean Drilling Program).

Lackschewitz, K.S., and Wallrabe-Adams, H.-J., 1991. Composition and origin of sediments on the mid-oceanic Kolbeinsey Ridge, north of Iceland. *Mar. Geol.,* 101:71–82.

Lackschewitz, K.S., Wallrabe-Adams, H.-J., and Garbe-Schönberg, D., 1994. Geochemistry of surface sediments from the mid-oceanic Kolbeinsey Ridge, north of Iceland. *Mar. Geol.,* 121:105–119.

Larsen, G., 1981. Tephrochronology by microprobe glass analysis. *In* Self, S., and Sparks, R.S.J. (Eds.), *Tephra Studies:* Dordrecht (Reidel Publ.), 95–102.

Le Bas, M.J., Le Maitre, R.W., Streckeisen, A., and Zanettin, B., 1986. A chemical classification of volcanic rocks based on the total alkali-silica diagram. *J. Petrol.,* 27:745–750.

Leg 151 Shipboard Scientific Party, 1995. Farthest north: ocean drilling in the Arctic Gateway region. *GSA Today,* 5.

Loebner, B., 1982. Petrology and source of volcanic ash layers in North Atlantic deep-sea sediments [M.S. thesis]. Univ. Rhode Island.

Maaløe, S., Sørensen, I., and Hertogen, J., 1986. The trachybasaltic suite of Jan Mayen. *J. Petrol.,* 27:439–466.

Meyer, O., Voppel, D., Fleischer, U., Closs, H., and Gerke, K., 1972. Results of bathymetric, magnetic and gravimetric measurements between Iceland and 70°N. *Dtsch. Hydrogr. Z.,* 25:193–201.

Meyer, P.S., Sigurdsson, H., and Schilling, J.-G., 1985. Petrological and geochemical variations along Iceland's neovolcanic zones. *J. Geophys. Res.,* 90:10043–10072.

Myhre, A.M., and Thiede, J., 1995. North Atlantic–Arctic Gateways. *In* Myhre, A.M., Thiede, J., Firth, J.V., et al., *Proc. ODP, Init. Repts.,* 151: College Station, TX (Ocean Drilling Program), 5–26.

Myhre, A.M., Thiede, J., Firth, J.V., et al., 1995. *Proc. ODP, Init. Repts.,* 151: College Station, TX (Ocean Drilling Program).

Nielsen, C.H., and Sigurdsson, H., 1981. Quantitative methods for electron microprobe analysis of sodium in natural and synthetic glasses. *Am. Mineral.,* 66:547–552.

Ninkovich, D., Sparks, R.S.J., and Ledbetter, M.T., 1978. The exceptional magnitude and intensity of the Toba eruption, Sumatra: an example of the use of deep-sea tephra layers as a geological tool. *Bull. Volcanol.,* 41:286–297.

O'Nions, R.K., Fridleifsson, I.B., and Jakobsson, S.P., 1973. Strontium isotopes and rare earth elements in basalts from the Heimaey and Surtsey volcanic eruptions. *Nature,* 243:213–214.

O'Nions, R.K., and Grönvold, K., 1973. Petrogenetic relationships of acid and basic rocks in Iceland: Sr isotopes and rare earth elements in late postglacial volcanics. *Earth Planet. Sci. Lett.,* 19:397–409.

O'Nions, R.K., Pankhurst, R.J., and Grönvold, K., 1976. Nature and development of basalt magma sources beneath Iceland and the Reykjanes Ridge. *J. Petrol.,* 17:315–338.

Oskarsson, N., Sigvaldason, G.E., and Steinthórsson, S., 1982. A dynamic model of rift zone petrogenesis and the regional petrology of Iceland. *J. Petrol.,* 23:28–74.

————, 1985. Iceland geochemical anomaly: origin, volcanotectonics, chemical fractionation and isotope evolution of the crust. *J. Geophys. Res.,* 90:10011–10025.

Sejrup, H.P., Sjøholm, J., Furnes, H., Beyer, I., Eide, L., Jansen, E., and Mangerud, J., 1989. Quaternary tephrachronology on the Iceland Plateau, north of Iceland. *J. Quat. Sci.,* 4:109–114.

Shackleton, N.J., Backman, J., Zimmerman, H., Kent, D.V., Hall, M.A., Roberts, D.G., Schnitker, D., Baldauf, J.G., Desprairies, A., Homrighausen, R., Huddlestun, P., Keene, J.B., Kaltenback, A.J., Krumsiek, K.A.O., Morton, A.C., Murray, J.W., and Westberg-Smith, J., 1984. Oxygen isotope calibration of the onset of ice-rafting and history of glaciation in the North Atlantic region. *Nature,* 307:620–623.

Shackleton, N.J., Berger, A., and Peltier, W.A., 1990. An alternative astronomical calibration of the lower Pleistocene timescale based on ODP Site 677. *Trans. R. Soc. Edinburgh: Earth Sci.,* 81:251–261.

Shipboard Scientific Party, 1995. Site 907. *In* Myhre, A.M., Thiede, J., Firth, J.V., et al., *Proc. ODP, Init. Repts.,* 151: College Station, TX (Ocean Drilling Program), 57–111.

Sigurdsson, H., 1971. Feldspar relations in Icelandic alkalic rhyolites. *Mineral. Mag.,* 38:503–510.

————, 1981. First-order major element variation in basalt glasses from the Mid-Atlantic Ridge: 29°N to 73°N. *J. Geophys. Res.,* 86:9483–9502.

Sigurdsson, H., and Loebner, B., 1981. Deep-sea record of Cenozoic explosive volcanism in the North Atlantic. *In* Self, S., and Sparks, R.S.J. (Eds.), *Tephra Studies:* Dordrecht (Reidel Publ.), 289–316.

Sigurdsson, H., Schilling, J.-G., and Meyer, P.S., 1978. Skagi and Langjökull volcanic zones in Iceland, 1. Petrology and structure. *J. Geophys. Res.,* 83:3971–3982.

Sigurdsson, H., and Sparks, R.S.J., 1981. Petrology of rhyolitic and mixed magma ejecta from the 1875 eruption of Askja, Iceland. *J. Petrol.,* 22:41–84.

Sjøholm J., Sejrup H.P., and Furnes, H., 1991. Quaternary volcanic ash zones on the Iceland Plateau, southern Norwegian Sea. *J. Quat. Sci.,* 6:159–173.

Sylvester, A.G., 1975. History and surveillance of volcanic activity on Jan Mayen island. *Bull. Volcanol.,* 39:1–23.

————, 1978. Petrography of volcanic ashes in deep-sea cores near Jan Mayen Island: Sites 338, 345–350, DSDP Leg 38. *In* Talwani, M., Udintsev, G., et al., *Init. Repts. DSDP,* Suppl. to 38, 39, 40, 41: Washington (U.S. Govt. Printing Office), 101–109.

Talwani, M., and Eldholm, O., 1977. Evolution of the Norwegian-Greenland Sea. *Geol. Soc. Am. Bull.,* 88:969–999.

Talwani, M., Udintsev, G., et al., 1976. *Init. Repts. DSDP,* 38: Washington (U.S. Govt. Printing Office).

Thompson, R.N., and MacKenzie, W.S., 1967. Feldspar-liquid equilibria in peralkali liquids: an experimental study. *Am. J. Sci.,* 265:714.

Vogt, P.R., Johnson, G.L., and Kristjansson, L., 1980. Morphology and magnetic anomalies north of Iceland. *J. Geophys.,* 47:67–80.

Walker, G.P.L., 1971. Grain-size characteristics of pyroclastic deposits. *J. Geol.,* 79:696–714.

Wells, S., Tadross, M., Garbett, D., and Shipboard Scientific Party, 1995. Sea ice observations log. *In* Myhre, A.M., Thiede, J., Firth, J.V., et al., *Proc. ODP, Init. Repts.,* 151: College Station, TX (Ocean Drilling Program), 423–452.

**Date of initial receipt: 30 June 1995**
**Date of acceptance: 3 December 1995**
**Ms 151SR-122**

**Table 4. Trace element analyses (ppm) of bulk ash layers from Hole 907A by neutron activation (INAA).**

| Core, section: | 1H-3 | 1H-3 | 1H-3 | 2H-3 | 3H-4 | 3H-4 | 3H-6 | 5H-4 | 6H-6 | 7H-4 | 7H-6 | 7H-6 | 7H-6 | 8H-1 | 8H-4 | 9H-2 | 9H-3 | 9H-4 | 9H-6 | 9H-6 |
|---|---|---|---|---|---|---|---|---|---|---|---|---|---|---|---|---|---|---|---|---|
| Interval (cm): | 53–55 | 61–63 | 71–73 | 97–99 | 47–49 | 52–54 | 118–120 | 36–38 | 111–113 | 86–88 | 120–122 | 131–133 | 137–139 | 1–3 | 39–41 | 39–41 | 35–37 | 52–54 | 64–66 | 102–104 |
| Layer: | C | D* | D* | E | H* | H* | I | K | L | N | Q | R* | R* | S | U | W | X | Y | Z | AA |
| Rb | 83 | 77 | 75 | 150 | 81 | 84 | 130 | 54 | 47 | 42 | 28 | 110 | 1.3 | 110 | 20 | 40 | | 43 | | 63 |
| Cs | 0.94 | 0.83 | 0.71 | 1.7 | 0.96 | 0.87 | 1.5 | 0.5 | 0.62 | 0.34 | 0.37 | 0.99 | 1.1 | 1.6 | 0.59 | 0.78 | | 0.8 | | 0.88 |
| Br | 3.2 | 2.3 | 2.8 | 3.8 | 4.3 | 3.2 | 7.4 | 4.2 | 2.4 | 1.2 | 3.8 | 3.5 | 4.1 | 4.4 | 3.2 | 3.4 | 1.1 | 0.65 | | 3.2 |
| Cr | 13 | 8.5 | 5 | 16 | 5.8 | 9.6 | 14 | 3.5 | 5.3 | 8 | 10 | 7.7 | 11 | 4.4 | 1.7 | 8.9 | 74 | 11 | 7.6 | 4.5 |
| Co | 3.1 | 6 | 7.2 | 4.2 | 5.1 | 6.5 | 6.4 | 26 | 4.6 | 8.3 | 26 | 2.2 | 2.1 | 1.5 | 38 | 3.7 | 39 | 3 | 38 | 1.5 |
| Ni | <40 | <80 | <40 | <40 | <20 | | | | | | | | | | | 21 | 42 | | 37 | 15 |
| As | <5.6 | 2.6 | 3.6 | 2.1 | 2.6 | <5.4 | <8 | 140 | 34 | 8.6 | 310 | 2.3 | 1.3 | 6.2 | 3.2 | 4.3 | 5.7 | 2.2 | 130 | 1.4 |
| Se | 9.8 | 16 | 19 | <2.2 | 16 | <1.9 | 23 | 120 | 9.2 | 7.4 | 2.8 | 18 | 19 | 11 | 2.8 | 10 | 2.5 | 5.9 | 2.7 | 9.6 |
| Sr | <40 | <100 | <100 | 250 | <60 | <60 | <0.6 | 210 | | | | | | | | 110 | 160 | 110 | 320 | 62 |
| Zr | 820 | 1200 | 1500 | 840 | 1100 | 1300 | 1100 | 830 | 420 | 670 | 280 | 540 | 580 | 330 | | 970 | 140 | 350 | 280 | 77 |
| Sb | 2.5 | 0.54 | 1.6 | 0.31 | 0.49 | 0.62 | 0.48 | 0.94 | 1.3 | 0.37 | 1.1 | 0.41 | 0.81 | 0.54 | 1.3 | 2.3 | 1.5 | 3.4 | 1.9 | 0.35 |
| Ba | 510 | 710 | 680 | 910 | 520 | 550 | 260 | 380 | 390 | 300 | 180 | 42 | 58 | 430 | 220 | 400 | <82 | 370 | 120 | 530 |
| Sc | 5.6 | 5.2 | 7.5 | 6 | 4.5 | 5.2 | 5.5 | 18 | 6.1 | 11 | 18 | 2.7 | 2.3 | 3 | 33 | 3.5 | 3.8 | 6.1 | 26 | 2.2 |
| La | 75 | 110 | 110 | 120 | 110 | 110 | 140 | 71 | 64 | 53 | 30 | 98 | 100 | 70 | 18 | 77 | 11 | 41 | 18 | 75 |
| Ce | 180 | 260 | 250 | 240 | 240 | 230 | 300 | 170 | 150 | 120 | 72 | 200 | 210 | 140 | 39 | 160 | 27 | 92 | 46 | 150 |
| Nd | 89 | 110 | 110 | 78 | 110 | 110 | 130 | 79 | 72 | 53 | 31 | 74 | 79 | 53 | 13 | 92 | <21 | 35 | 17 | 70 |
| Sm | 17 | 22 | 22 | 11 | 20 | 21 | 22 | 17 | 13 | 12 | 8.8 | 10 | 11 | 8.2 | 3.5 | 16 | 4.4 | 11 | 6.9 | 14 |
| Eu | 8.2 | 6.2 | 6.3 | 3.2 | 4.2 | 4.2 | 4.8 | 4.8 | 2.7 | 2.8 | 2.4 | 2 | 2.2 | 0.9 | 11.3 | 4.3 | 1.7 | 2.1 | 2.5 | 2.9 |
| Tb | 2.7 | 3.5 | 3.2 | 1.1 | 3.3 | 3.1 | 3.2 | 2.5 | 1.8 | 2.2 | 1.2 | 1.1 | 1.1 | 1.1 | 1.4 | 2.5 | 1.1 | 2.1 | 1.2 | 2.2 |
| Yb | 9.9 | 11 | 11 | 4.8 | 12 | 12 | 13 | 9.2 | 8.5 | 7.9 | 5.1 | 3.8 | 4 | 4.4 | 2.2 | 8.4 | 2.9 | 8.4 | 3.5 | 7.9 |
| Lu | 1.4 | 1.5 | 1.5 | 0.66 | 1.6 | 1.6 | 1.9 | 1.3 | 1.2 | 1.15 | 0.77 | 0.54 | 0.56 | 0.64 | 0.36 | 1.2 | 0.43 | 1.2 | 0.52 | 1.1 |
| Hf | 19 | 25 | 25 | 16 | 23 | 24 | 24 | 18 | 12 | 15 | 9.2 | 10 | 11 | 8 | 2.4 | 20 | 3.7 | 8.7 | 6.6 | 16 |
| Ta | 5.7 | 11 | 9.9 | 71 | 8.4 | 8.3 | 13 | 5.7 | 4.8 | 3.9 | 2 | 10 | 11 | 5.9 | 1.8 | 5.8 | 0.87 | 3.2 | 1.4 | 5.5 |
| Th | 9.8 | 14 | 13 | 15 | 14 | 14 | 15 | 8.3 | 8.9 | 8.3 | 4.2 | 12 | 13 | 1.4 | 2.3 | 9.5 | 0.95 | 8.1 | 1.8 | 11 |
| U | 1.7 | 2.9 | 2.6 | 3.1 | 3.1 | 2.7 | 3.7 | 1.4 | 2.2 | 1.8 | 0.77 | 2.9 | 3.1 | 3.7 | <0.2 | 2.3 | 0.4 | 1.9 | <0.54 | 2.4 |

Notes: * = ash layer sampled at two depth intervals. <40 = below the detection limit.

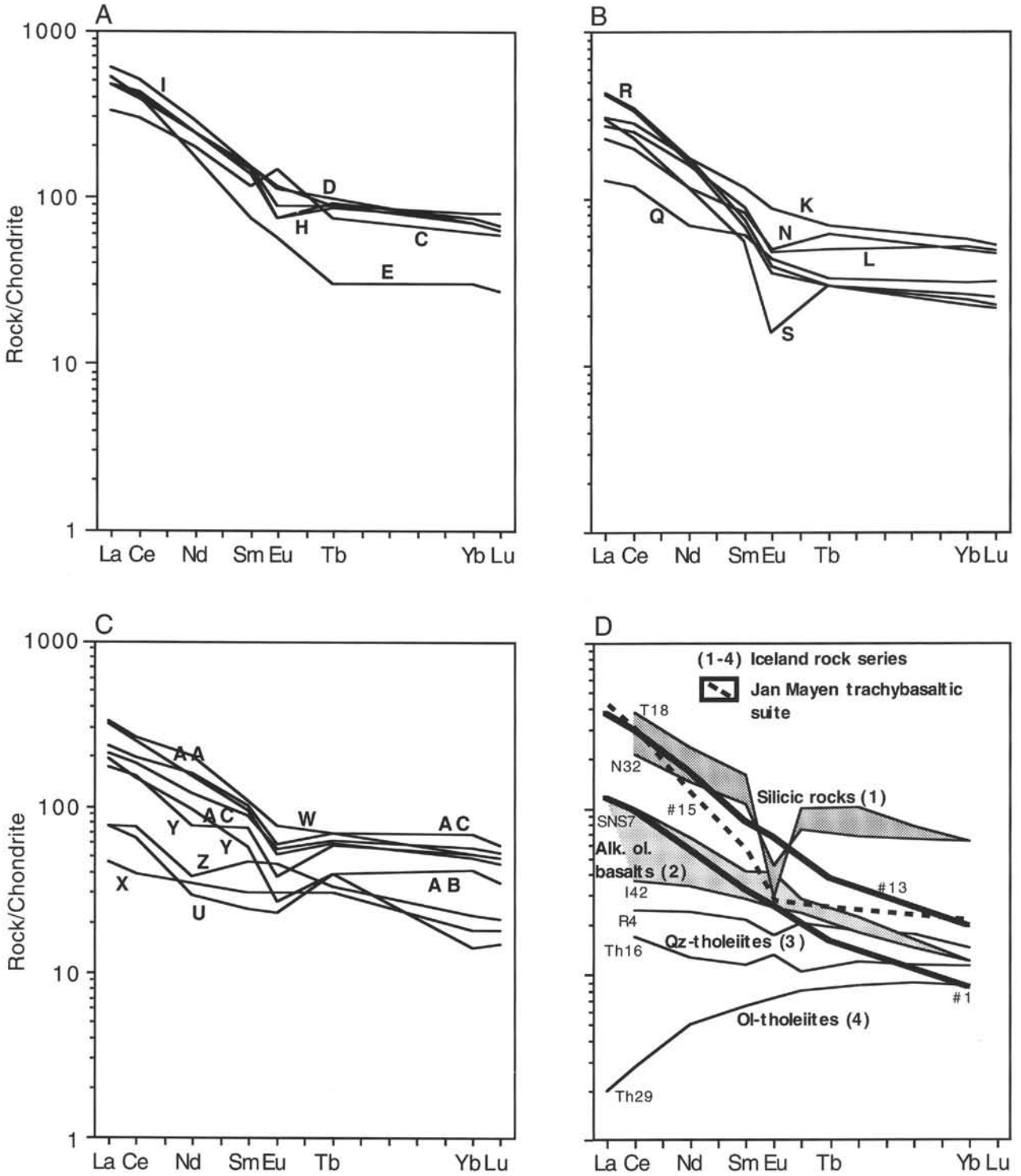


Figure 13. Chondrite-normalized REE diagrams for (**A**) Pleistocene, (**B**) late Pliocene, and (**C**) early Pliocene bulk ash analyses from Site 907. **D.** REE patterns of Icelandic and Jan Mayen volcanics (modified from Oskarsson et al., 1982; Maaløe et al., 1986). The data are taken from O'Nions and Grönvold (1973), O'Nions et al. (1973, 1976) for Iceland (analyses T18, N32, SNS7, I42, R4, Th16, and Th29), and from Maaløe et al. (1986) for Jan Mayen (analyses 1, 13, and 15). Normalization values according to Anders and Grevesse (1989).